Evaluation of the Surface Urban Energy and Water balance Scheme (SUEWS) at a dense urban site in Shanghai: sensitivity to anthropogenic heat and irrigation

Article

Accepted Version

Evaluation of the Surface Urban Energy and Water balance Scheme (SUEWS) at a dense urban site in Shanghai: Sensitivity to anthropogenic heat and irrigation

Xiangyu Ao[1,2,3,5], C.S.B. Grimmond[3], H.C. Ward[3], A.M. Gabey[3], Jianguo Tan[4,5], Xiu-Qun Yang[1**], Dongwei Liu[2,5], Xing Zhi[6], Hongya Liu[7], Ning Zhang[1*]

[1] School of Atmospheric Sciences, Nanjing University, China
[2] Shanghai Institute of Meteorological Science, China
[3] Department of Meteorology, University of Reading, UK
[4] Shanghai Climate Centre, Shanghai Meteorological Service, China
[5] Shanghai Key Laboratory of Meteorology and Health, China
[6] Department of Science and Technology Development, Shanghai Meteorological Service, China
[7] Shanghai Central Meteorological Observatory, China

*Corresponding authors E-mail: ningzhang@nju.edu.cn;
**Co-Corresponding authors E-mail: xqyang@nju.edu.cn

Abstract
The Surface Urban Energy and Water balance Scheme (SUEWS) is used to investigate the impact of anthropogenic heat flux (Q_F) and irrigation on surface energy balance partitioning in a central business district of Shanghai. Diurnal profiles of Q_F are carefully derived based on city-specific hourly electricity consumption data, hourly traffic data and dynamic population density. Q_F is estimated to be largest in summer (mean daily peak 236 W m^{-2}). When Q_F is omitted, the SUEWS sensible heat flux (Q_H) reproduces the observed diurnal pattern generally well, but the magnitude is underestimated compared to observations for all seasons. When Q_F is included, the Q_H estimates are improved in spring, summer and autumn, but poorer in winter indicating winter Q_F is overestimated. Inclusion of Q_F has little influence on the simulated latent heat flux (Q_E), but improves the storage heat flux estimates except in winter. Irrigation, both amount and frequency, has a large impact on Q_E. When irrigation is not considered, the simulated Q_E is underestimated for all seasons. The mean summer daytime Q_E is largely overestimated compared to observations under continuous irrigation conditions. Model results are improved when irrigation occurs with a 3-day frequency, especially in summer. Results are consistent with observed monthly out-door water use. This study highlights the importance of appropriately including the Q_F and irrigation in urban land surface models - terms not generally considered in many previous studies.

1. Introduction

China has experienced unprecedented urban growth in recent decades, with the fraction of city dwellers increasing from 17.9% to 55.6% between 1978 and 2015 (UN, 2017). If these rates continue, the urban population will exceed 1 billion in China within the next two decades. This rapid urbanization has brought significant economic growth, while at the same time exposing people to urban climatic and environmental risks, such as persistent heat waves, flooding and air pollution (Jiang et al. 2015; Li et al. 2015; Zhong et al. 2015; Ding et al. 2016; Xu et al. 2016; Yang et al. 2017). Cities are well known to have distinct climatic conditions that result from the alteration of the urban surface-atmosphere energy and water exchanges compared to surrounding rural surfaces (Roth et al. 2017; Zou et al. 2017). Absorption and trapping of incoming short-wave radiation by deep urban canyons leads to greater absorption of energy by the surface and a smaller surface albedo than surrounding environments (Oke 1988; Christen and Vogt 2004; Guo et al. 2016). More heat is stored in high thermal admittance building walls during the day-time, which is then released at night creating the distinct nocturnal urban heat island (UHI) (Grimmond and Oke, 1999; Roberts et al. 2006; Wu and Yang, 2013; Kotthaus and Grimmond, 2014). The replacement of natural vegetative surfaces with impervious paved and built surfaces leads to less energy partitioning into evapotranspiration and reduces the associated cooling effect (Grimmond and Oke 1986; Nakayoshi et al. 2009; Ward and Grimmond 2017). Urban runoff is usually significantly enhanced following rainfall, given the abundance of paved and built surfaces. This rapid rate of runoff also removes a large amount of surface water suppressing evaporation rates (Ragab et al. 2003). Human activities, related to building heating and cooling, vehicles and human metabolism (Sailor 2011; Lindberg et al. 2013) release extra anthropogenic heat into the urban environment.

Urban land surface models (ULSMs) can be effective tools to investigate and quantify these surface-atmosphere exchanges and interactions to yield insight into the different factors influencing the climate of a city. Numerous ULSMs have been developed over the last few decades, with varying degrees of complexity (e.g. Kusaka et al. 2001; Oleson et al. 2008; Järvi et al. 2011; Masson et al. 2013; Miao and Chen 2014). Grimmond et al. (2010; 2011), in the first international comparison of ULSMs, found no single model performs best or worst for all fluxes. Considering the implications of this study, Best and Grimmond (2016b) concluded that attention needs to be directed to the modelling of the latent heat flux, inclusion (or not) of vegetation, and calculation of the anthropogenic heat flux by ULSMs. These elements are simulated poorly, yet are key factors impacting overall model performance. They are the focus of this paper.

ULSMs often simulate the latent heat flux separately for natural (vegetation or pervious) and built (road, walls, roof) surfaces, with no interaction between them. Furthermore, ULSMs rarely incorporate any detailed consideration of urban hydrological processes, such as drainage, interception, runoff or irrigation. For example, the early version of the widely implemented SLUCM system (Kusaka et al. 2001) uses a simplified hydrologic process in which evaporation only occurs after precipitation events, even though SLUCM implements a sophisticated representation of urban canopy geometry. Recently, enhanced hydrological processes including anthropogenic latent heat, urban irrigation and urban oasis effects have been implemented into SLUCM system (Miao and Chen 2014; Yang et al. 2015), which improves the model performance substantially especially for the latent heat flux.

Given the large fraction of impervious surfaces in urban areas, city drainage systems are designed to quickly remove runoff. In many settings this gives rise to a deficit of soil moisture in the urban landscape (Coutts et al. 2013) and irrigation is often needed to maintain vegetation health (Grimmond and Oke 1986, Demuzere et al. 2014). This urban irrigation has been shown to be a critical component of the urban water balance, especially in arid and hot regions, and plays a key role in the energy partitioning between latent and sensible heat fluxes and the associated urban cooling efficiency. Vahmani and Hogue (2014, 2015) developed and assessed an irrigation scheme within the framework of the Noah/SLUCM system for the Los Angeles metropolitan area and demonstrated that appropriately incorporating urban irrigation can significantly improve model performance. However, the majority of ULSMs applications still ignore irrigation, especially in subtropical cities which are considered to have plenty of rainfall to maintain sufficient water supply. This, however, is not always the case, and with increased frequency of extreme heat waves the potential need for external water supply can be substantial in these cities.

The anthropogenic heat flux (Q_F) also plays a critical role in ULSMs and has been the focus of significant attention (Grimmond 1992; Sailor and Lu 2004; Allen et al. 2011; Zhang et al. 2015; Best and Grimmond 2016a). Q_F, the additional energy produced by human activities released into the environment, can be a significant component of the urban energy balance with distinct seasonal and diurnal variations. For example, the estimated daytime Q_F in central Tokyo (Ichinose et al. 1999) exceeded 400 W m^{-2} at 2 p.m. on average and reached 1590 W m^{-2} in winter (25 m resolution), enhancing the UHI by 1-2.5 °C. The magnitude of Q_F is scale and location dependent. Typically, it is highest in central urbanized areas and much less when averaged over the entire city. Incorporating Q_F into meso-scale weather forecast models has been shown to have a significant impact on model predictions when city specific Q_F profiles and magnitudes are provided (Salamanca et al. 2014). However, such city specific Q_F diurnal profiles are often very difficult to obtain given the lack of detailed local energy consumption data. As a result, most urban modellers simply use a default fixed Q_F diurnal profile (e.g. two diurnal peaks at 0800 and 1700 LST is the default in WRF/UCM), fixed values regardless of the city (e.g. Wang et al. 2015; Chen et al. 2016b), or turn anthropogenic heating off (e.g. Zhang et al. 2010; Loridan et al. 2013; Wang et al. 2013; Zhong et al. 2017). This diversity of approaches has contributed to contradictory results on the impact of Q_F on local climate. For example, two recent studies have shown inconsistent impacts of Q_F with the WRF/UCM default Q_F on precipitation: Chen et al. (2016a) report it results in increases in precipitation, while Feng et al. (2012) report a decrease of precipitation in the same region (Hangzhou, China). Others, however, have made significant advances in this realm. Sailor et al. (2015) developed a national database of anthropogenic heat profiles for the USA and extended this, by simple adjustments, for a range of international megacities. Adopting a different approach, Nie et al. (2017) used WRF/BEP-BEM to estimate spatially and diurnally varying Q_F in Beijing. However, given the vast diversity of cities in China, there is an urgent need to develop datasets and models that simulate the spatial and temporal variability of Q_F across cities.

The Surface Urban Energy and Water balance Scheme (SUEWS) is a local scale urban land surface model of moderate complexity (Järvi et al. 2011; Ward et al. 2016). SUEWS has the advantage that it simulates the urban surface energy balance in combination with the complete urban hydrological cycle, considering irrigation and runoff processes. The urban water balance interacts with the energy balance through evaporation E, as $Q_E=L_VE$, where Q_E is the latent heat flux and L_V is the latent heat of vaporization. Moreover, SUEWS requires only commonly available meteorological input data and detailed information about the urban surface. The urban surface is split into seven land cover types (buildings, paved surfaces, coniferous trees and shrubs, deciduous trees and shrubs, grass, bare soil and water) with integrated urban vegetation effects, a previously highlighted key factor for improving the accuracy of ULSMs (Grimmond et al. 2010, 2011). These characteristics of SUEWS have enabled the model to be used widely as an effective tool for climate (water) sensitive urban design, and urban climate disaster and mitigation strategy assessment (Mitchell et al. 2008; Järvi et al. 2017; Ward et al. 2017a, b; Rafael et al. 2017).

The SUEWS model was originally tested using data collected from a mid-latitude suburb in Vancouver, Canada (Grimmond et al. 1986; Grimmond and Oke 1991; Loridan et al. 2011; Järvi et al. 2011). It has been evaluated extensively in North American and European cities and shown to produce realistic and robust results (Järvi et al. 2014; Alexander et al. 2015; Karsisto et al. 2016; Ward et al. 2017a; Kokkonen et al. 2018). However, evaluation of SUEWS in rapidly urbanizing subtropical (or tropical) cities is still lacking, with the exception of recent work in tropical Singapore (Demuzere et al. 2017). Given the vast diversity of climatic settings and urban geometrical structures (cf. Local Climate Zones, Stewart and Oke 2012) of different cities, further evaluation of the model in subtropical cities is of paramount importance. Shanghai, the largest subtropical city in China, characterized by numerous sky-scrapers and dense urbanization, provides a test-bed to evaluate SUEWS.

The objective of this study is to evaluate the performance of SUEWS in a central business site of Shanghai for one year using directly measured surface energy flux observations (Ao et al. 2016a, b). Special attention is directed to the impact of the seasonally varying diurnal profiles of Q_F derived from city scale annual energy consumption data, hourly electricity power load data, and traffic count data. The impact of urban irrigation on the simulation of latent heat flux (evaporation) is also addressed using the empirical irrigation scheme in SUEWS. This study provides insights into the performance of SUEWS and its potential to investigate strategies to mitigate urban heat stress and create resilient and sustainable urban environments.

2. Methodology

2.1 Site and Observations

The evaluation of SUEWS uses data (December 2012 – November 2013) observed over a dense urban site ('XJH') in Shanghai, China (Fig. 1). The four components of net all-wave radiation, the turbulent sensible and latent heat fluxes, along with basic meteorological variables (air temperature, relative humidity and pressure) are directly measured at this site on a tall tower (full details are provided in Ao et al. 2016a, b). Precipitation is measured nearby (60 m away) with an automatic weather station (AWS).

Annual and seasonal performance of SUEWS is considered using carefully quality controlled data (see further details in Ao et al., 2016a, b). Data from sectors strongly influenced by a tall building (210-247°) and the tower itself (320-337°) are excluded. Wet conditions (within 1 day after rain) are excluded as rain drops on open-path sensors generate errors.

Surface cover parameters needed for SUEWS are retrieved from GIS data and a ground survey for a 500 m radius around the site. The Kljun et al. (2004) flux source area model suggests that the 80% source area extends to about 600 m from the site.

The four seasons of a year are defined based on the commonly used classification in China: winter [December–February (DJF)], spring [March–May (MAM)], summer [June–August (JJA)], and autumn [September–November (SON)]. Local standard time is used (China does not use day light savings time).

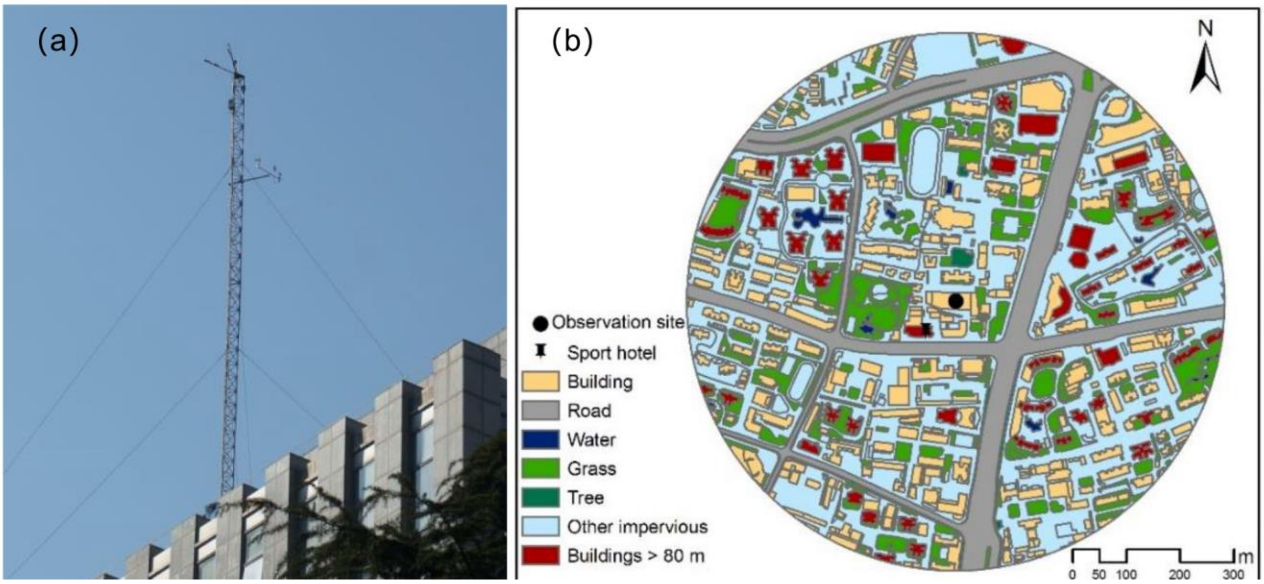

Figure 1: Study site (XJH) in Shanghai: (a) flux tower, and (b) land cover within 500 m (see Fig. 1 in Ao et al. 2016a).

2.2 Estimation of anthropogenic heat flux (Q_F)

In SUEWS, the daily anthropogenic heat flux ($Q_{F,S,daily}$) is calculated adopting the Sailor and Vasireddy (2006) based approach. This is a function of population density (ρ_{pop}) and heating and cooling degree days (*HDD* and *CDD*) (Fig. 2a):

$$Q_{F,S,daily} = \rho_{pop}\,[a_{F0} + a_{F1}\,CDD + a_{F2}\,HDD] \tag{1}$$

with daily *HDD* and *CDD* defined based on the hourly air temperature (T_i) and a balance point temperature (T_b) for human comfort, as:

$$HDD = \sum_{i=1}^{24}(T_b - T_i)l$$
$$CDD = \sum_{i=1}^{24}(T_i - T_b)l \tag{2}$$

Logic variable (l) equals 1 when (T_b-T_i) > 0 °C and equals 0 when (T_b-T_i) < 0 °C for HDD, and vice versa for CDD; and a_{F0} is the base $Q_{F,S,daily}$ from all sources at the balance point temperature. The slopes a_{F1} and a_{F2} differ (Fig. 2a). Three coefficients (a_{F0}, a_{F1}, a_{F2}) need to be specified for a study site. Here daily results ($Q_{F,L,daily}$) from LQF (Appendix A) is used to obtain these three coefficients. The fitted cooling slope (a_{F1}) is 0.0181 W m^{-2} K^{-1} (capita ha^{-1})$^{-1}$, the heating slope (a_{F2}) is 0.0035 W m^{-2} K^{-1} (capita ha^{-1})$^{-1}$, and a_{F0} = 0.3963 W m^{-2} (capita ha^{-1})$^{-1}$ with the single T_b of 20 °C.

The diurnal profiles of the building Q_{FB} for weekday, weekend and holidays (Fig. 3a) are mainly based on diurnal variations of the city-scale electricity consumption data and further scaled by electricity fraction of Shanghai (14%, Table 1), industry fraction of XJH site (10%) and diurnal variation of population density (Yu and Wen (2016); Zhong et al. 2017). The diurnal profiles of the vehicle based Q_{FB} (Fig. 3b) are derived from hourly highway traffic data for the inner ring of Shanghai in 2011 (Su et al. 2014) (see section 3.1 and Appendix A).

Table 1: Energy consumption in Shanghai (Shanghai Municipal Statistics Bureau 2016) in tonne coal equivalent (TCE) is converted to kWh assuming 1 TCE=8141 kWh (Kyle's Converter 2017).

Year	Energy consumption 10^4 TCE		Electricity consumption 100 million kWh		Electricity consumption 10^4 tons SCE	f_{ele}	N_{pop} 10^4 persons
	Total	Industry	Total	Industry			
2005	7974.24	4863.17	921.97	617.59	1133.10	0.1421	1890.26
2006	8604.89	5152.05	990.15	656.1	1216.89	0.1414	1964.11
2007	9374.6	5452.95	1072.38	705.9	1317.96	0.1406	2063.58
2008	9894.52	5598.41	1138.22	727.13	1398.87	0.1414	2140.65
2009	10050.06	5465.53	1153.38	701.59	1417.50	0.1410	2210.28
2013	11345.69	6009.41	1410.61	799.45	1733.64	0.1528	2415.27

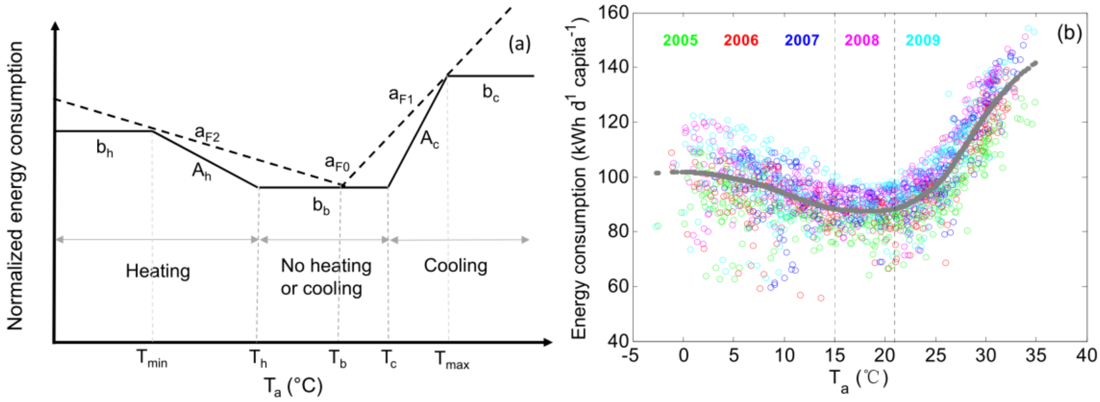

Figure 2: Energy consumption response to air temperature: (a) two general response functions (see text for definitions); and (b) data for Shanghai (whole city daily electricity consumption) (kWh d^{-1} capita^{-1}) (Shanghai Electric Power Company, Liu and Cao 2013) normalized by population (Shanghai Municipal Statistics Bureau 2016) and XJH daily mean air temperature (T_a) for 2005-09 with general trend (grey, loess curve).

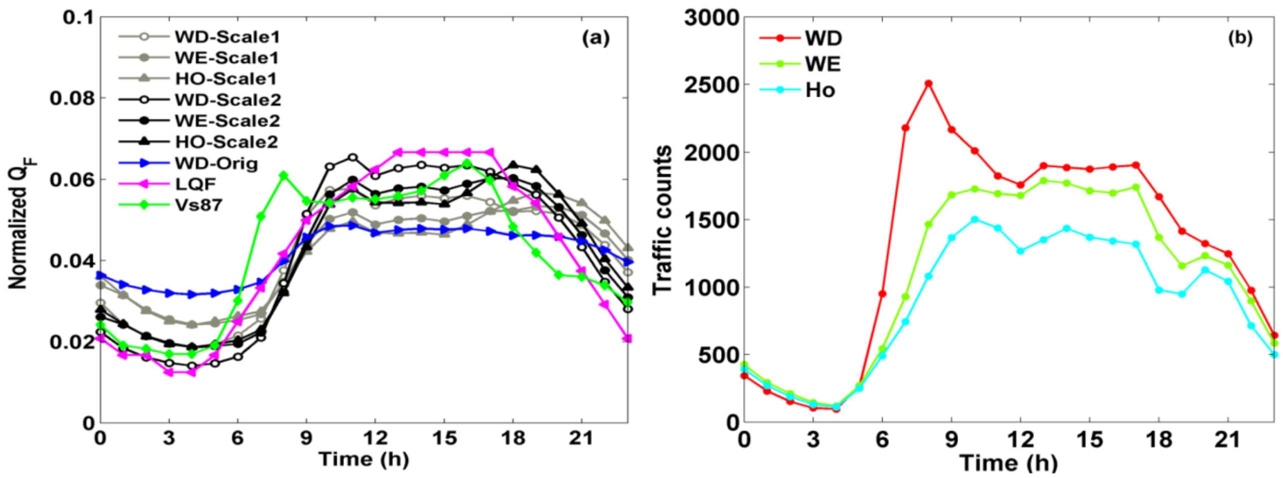

Figure 3: Diurnal profiles for weekdays (WD), weekends (WE) and holidays (HO) of (a) building anthropogenic heat flux at the XJH site with 10% urban industry fraction used (scale 1), with variation of population density accounted for (scale 2), plus weekdays China LQF (Allen et al. 2011) and Vs87 (Grimmond 1992, Järvi et al. 2011) profiles; and (b) traffic counts for highways near XJH in 2011 (Su et al. 2014; Shanghai Road Administration Bureau).

2.3 Estimation of Irrigation

Irrigation and street cleaning provides additional water to precipitation for runoff, evaporation and soil moisture storage. In areas dominated by impervious surfaces, with limited available water for evaporation, the impact can be significant (Best and Grimmond 2016b; Sun et al. 2014). In SUEWS, the probable daily external water use (I_e) is calculated as a function of the daily mean air temperature (T_d) and number of days after rain (D_{ar}) (Järvi et al. 2011):

$$I_e = \sum_{iv=1}^{3} f_{iv}[f_{aut}(b_{0,a} + b_{1,a}T_d + b_{2,a}D_{ar}) + (1 - f_{aut})(b_{0,m} + b_{1,m}T_d + b_{2,m}D_{ar})] \qquad (3)$$

For each of the *iv* vegetation types the irrigation fraction (f_{iv}) and its method (automatic f_{aut} or manual) are needed. The site specific coefficients ($b_{0,a}$, $b_{1,a}$, $b_{2,a}$ *and* $b_{0,m}$, $b_{1,m}$, $b_{2,m}$) characterize the behaviour of automated (*a*) and manual (*m*) irrigation during the period of external water use ($I_{e,start}$ and $I_{e,end}$, days of year). The parameters used are given in Table 2. Additionally, days of week when irrigation is permitted need to be specified (Shanghai: no restricted days of week). With the user provided diurnal profiles of water use (see section 3.4.1), the daily irrigation is downscaled to hourly and then 5 min.

2.4 SUEWS model setup and parameters

Version v2017a of SUEWS (Ward et al. 2016, 2017a, b) is used with a 5 min time-step but forced by 60 min meteorological input data. The incoming shortwave radiation flux ($K\downarrow$), air temperature (T_a), pressure (p), relative humidity (RH) and precipitation (P), are linearly interpolated to 5 min by SUEWS. The 60 min averaged (by SUEWS) output are used in the comparison with observations. The parameter values used to characterise the study site (XJH) are given in Table 2.

Surface cover and mean building height (z_H) parameters are derived from GIS and ground survey data (Ao et al. 2016a). The roughness length (z_0) and the zero-plane displacement height (z_d) method selected is the simple fixed fraction of the mean building height (z_H) or rule-of-thumb (0.1 z_H and 0.7 z_H) (Grimmond and Oke 1999). Given the conclusions of Kent et al. (2017) and Tang et al. (2016), runs are also undertaken using Kanda et al. (2013) method. Mean values calculated around the site (1° interval) gave z_0=7.6 and z_d=55 m. The model result difference from that of rule-of-thumb method is small (not shown).

The leaf area index (LAI) or phenology has a critical influence on the latent heat flux (Q_E) and timing of appropriate seasons. It dynamically responds to growing degree days (*GDD*) and senescence degree days (*SDD*). Phenology parameters are determined from observations and photographs with local daily mean air temperatures (leaf-on ($T_{base-on}$), leaf-off ($T_{base-off}$), growing degree days until full LAI (GDD_{full}) and senescence degree days that initiate leaf off (SDD_{full}) are calculated as cumulative values of *GDD* and *SDD* during growing and senescence periods in Shanghai (around 15 March – 20 May, 15 October – 20 December, respectively). The equation used for *GDD* (*SDD*) in SUEWS is (McMaster and Wilhelm 1997):

$$GDD=[(T_{max}+T_{min})/2] - T_{base-on}$$
$$SDD=[(T_{max}+T_{min})/2] - T_{base-off} \qquad (4)$$

where T_{max} and T_{min} are daily maximum and minimum air temperature, respectively. *GDD* (*SDD*) must be greater (smaller) than 0, if not, they are forced to 0. As expected, the Shanghai $T_{base-on}$ and $T_{base-off}$ (10 °C and 20 °C, Table 2) are much warmer than for Helsinki and Montreal (5 °C and 10 °C, Järvi et al. 2014) and London (6 °C and 11 °C, Ward et al. 2016). Latitude strongly impacts the length of growing (senescence) season. The daily *LAI* for each vegetation type (*iv*) is a function of the previous day LAI ($LAI_{d-1,iv}$), daily mean air temperature (T_d) and day length (t_d) (Järvi et al. 2014). For leaf on, $T_d > T_{base-on}$

$$LAI_{d,iv} = LAI_{d-1,iv}^{c_1} GDD \cdot c_2 + LAI_{d-1,iv} \qquad (5a)$$

For leaf off, it may be initiated by a thermal condition only ($T_d < T_{base-off}$)

$$LAI_{d,iv} = LAI_{d-1,iv}^{c_3} SDD \cdot c_4 + LAI_{d-1,iv} \qquad (5b1)$$

or also account for day length (t_d < 12 h)

$$LAI_{d,iv} = LAI_{d-1,iv} c_3 SDD \cdot c_4 + LAI_{d-1,iv} \qquad (5b2)$$

From sensitivity experiments (not shown), it is found that accounting for day length (Eq. 5b2) is unsuitable at this subtropical site (small variation of t_d) as simulated leaf-off occurs too early and the senescence is too fast. Hence Eq. 5b1 is adopted in this study. The parameters $c_{1,2,3,4}$ control the changing rate of *LAI*. $c_{1,2,3}$ parameters values are the same in Järvi et al. (2014) for Helsinki. While c_4 for evergreen trees a smaller value is used based on local visual/photograph surveys that leaves are still partially active to late December. The subtropical climate and careful maintenance (e.g. turf replacement if it turns yellow) at the Shanghai site results in a longer growing season for grass than higher latitudes. Based on photographs taken around the XJH site in winter and spring (not shown), the grass remains green in winter months. Therefore, the minimum *LAI* for grass is increased from 1.6 in (Järvi et al. 2014) to 3.2 at our site (Table 2) which results in a better model performance especially in winter and spring seasons (not shown).

Previous evaluation of the radiation components of SUEWS (Ao et al. 2016b) found good performance. The net all-wave radiation flux (Q^*) modelled with downward long wave radiation flux ($L_\downarrow$) estimated as a function of *RH* and T_a. The storage heat flux is calculated using the objective hysteresis model (OHM, Grimmond et al. 1991), with (Q^*+Q_F) (rather than only Q^*) used:

$$\Delta Q_S = \sum_i f_i \left[a_{1i}(Q^* + Q_F) + a_{2i}\frac{\partial(Q^*+Q_F)}{\partial t} + a_{3i}\right] \qquad (6)$$

where f_i is the fraction for the i_{th} surface type, and *t* is the time. The three coefficients (a_1, a_2, a_3) of OHM are from the literature (Table 2).

The latent heat flux (Q_E) is modelled using the modified Penman-Monteith equation (Grimmond and Oke, 1991). More detailed description of the parameterization of Q_E is given in section 3.3. The sensible heat flux (Q_H) is calculated as a residual of the surface energy balance. The soil layer underneath each surface type (except water surface) is assumed to be 350 mm, with a maximum water capacity of 150 mm. To obtain appropriate initial conditions, SUEWS is run for one year with the 2012/2013 forcing to get probable initial state of soil moisture storage and leaf area index.

3. Results

3.1 Anthropogenic heat fluxes

The diurnal profiles of the building anthropogenic heat flux for weekdays, weekends and holidays are similar (Fig. 3a): all are low from midnight to 06:00, then increase gradually until 11:00, with a small decrease at 12:00. Thereafter, the three diurnal patterns begin to diverge. During weekdays values remain relatively constant from 12:00 to 17:00, then decrease steadily. During weekends the timing of this decrease lags by 2 hours (i.e. from 19:00), whereas on holidays there is a stronger evening peak around 19:00.

The diurnal profiles that account for population variations (Fig. 3a) have much larger amplitudes than the original profiles and are similar in amplitude to the default LQF and SUEWS Vs87 profiles (Grimmond 1992; Järvi et al. 2011) and to other studies, for example in Japan (Takane et al. 2017). The ratios of the maximum and minimum value for scaled weekday, weekend and holiday are 4.7, 3.2 and 3.4, respectively. The corresponding values for LQF and SUEWS Q_F scheme are 5.3 and 3.8, respectively.

Seasonal differences in diurnal patterns and magnitudes of the vehicle heat emissions are relatively small (not shown). The weekday morning peak (at 08:00) is distinct whereas the evening peak (at 17:00) (Fig. 3b) is unlike North American cities where the evening peak is generally stronger than the morning peak (Grimmond 1992; Hallenbeck et al. 1997; Chow et al. 2014). This may be because the end of work varies between companies, while most institutions or government offices finish between 17:00-18:00 but many people often stay at the office in the evening. Additionally, shopping malls and restaurants are open until 21:00 - 22:00. The weekend pattern, without distinct peaks, slowly increases in the morning then stays flat from about 10:00 - 17:00. Holidays have a similar pattern to the weekend but with smaller magnitudes.

The LQF and SUEWS Q_F results are very similar (Fig. 4). As the three SUEWS coefficients (a_{F0}, a_{F1}, a_{F2}) are derived using the LQF results, this is expected. The larger summertime results are a function of the larger a_{F2} slope and therefore dependence on *CDD*, as expected. The peak mean daily summer $Q_{F,L}$ (Fig. 4) is around 236 W m^{-2}; winter and autumn mean fluxes peak are similar (190 W m^{-2}) and spring slightly smaller (180 W m^{-2}). These values, using the new response function, give a slightly bigger seasonal variation that the original function (not shown). The building heat emission is the major sub-component, accounting for about 95% of the total $Q_{F,L}$. The modelled metabolic heat emission (Q_{FM}) is about 3 W m^{-2} at night and 7 W m^{-2} during daytime and does not show seasonal variations. Seasonal differences in vehicle heat emissions also are very small, with Q_{FV} around 3 W m^{-2} in the daytime. The small (or no) seasonal variation for Q_{FV} and Q_{FM} is because the same parameter settings assumed for each season as there is a lack of information to suggest otherwise. The difference between winter and the other three seasons is because more holidays occur in winter. The magnitudes of Q_{FM} and Q_{FV} estimated here are similar to previous studies (Chow et al. 2014; Lu et al. 2016; Stewart and Kennedy 2016). There is a high correlation coefficient (0.97) between hourly $Q_{F,S}$ and $Q_{F,L}$. Given the simplicity of SUEWS Q_F, the dynamic temperature response, and comparable results to LQF, the SUEWS Q_F is regarded as an appropriate method to use after careful determination of the parameters. As the purpose of this study is the evaluation of SUEWS, the SUEWS Q_F are used in the following sections.

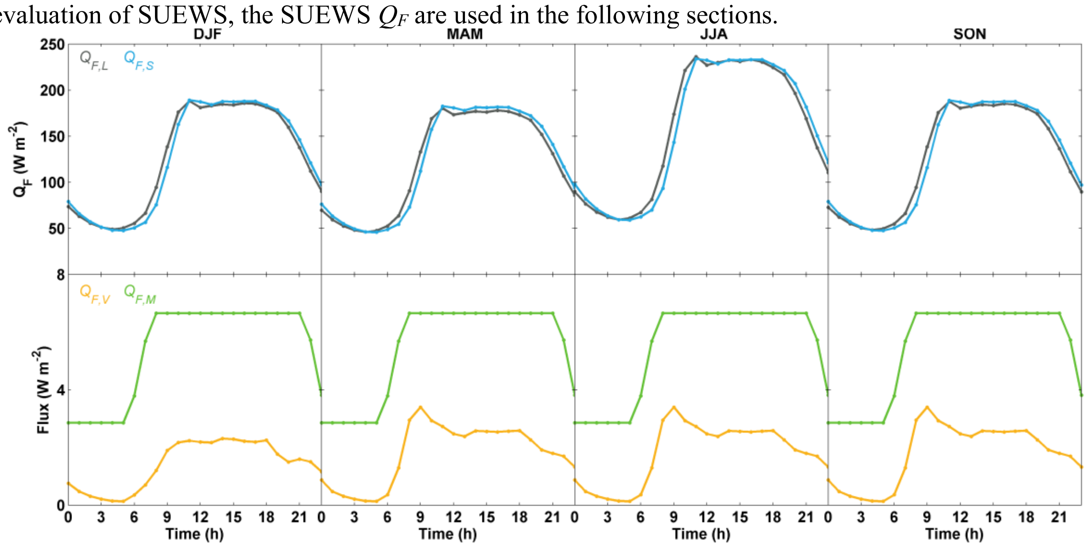

Figure 4: Seasonal mean diurnal variations of Q_F at XJH estimated by LQF and SUEWS (section 2.2), LQF metabolic heat ($Q_{F,M}$) and vehicle heat ($Q_{F,V}$) emissions.

3.2 Impact of Q_F on surface energy fluxes

Two simulations to examine the impact of Q_F on the surface energy balance fluxes in Shanghai are conducted (Figures 5, C.1, C.2, C.3): i) assuming $Q_F = 0$ W m^{-2} (hereafter $Q_{F,0}$ *Noirr*) and (ii) using SUEWS determined flux ($Q_{F,S}$ *Noirr*). No irrigation is considered in these two simulations (*Noirr*).

When $Q_{F,0}$ is assumed, the turbulent sensible heat flux (Q_H) is generally underestimated (negative *MBE*) for the four seasons, especially during afternoon and midnight. Including Q_F leads to a large increase in Q_H. The seasonal mean diurnal Q_H is overestimated through the entire day in winter, spring and autumn, while in summer daytime Q_H is slightly underestimated and nocturnal Q_H is overestimated (Fig. 5). The *MBE* for the four seasons are all positive when $Q_{F,S}$ is used (Table 3). The overall performance for Q_H is improved in spring, summer and autumn with RMSE decreased (-7, -33 and -12 W m^{-2}, respectively). The coefficient of determination (R^2) increases slightly in spring and summer for the $Q_{F,S}$ case. But the *RMSE* and *MBE* increase in winter, suggesting winter Q_F may be overestimated.

Given the complex sampling issues, direct measurements of the storage heat flux (ΔQ_S) in an urban area with a wide range of tall 3-D volumes has not been undertaken. Instead, the "observed" ΔQ_S is estimated as the residual of the surface energy balance ($\Delta Q_S = Q^* + Q_F - Q_H - Q_E$), therefore including considerable uncertainties. As a result, the observed ΔQ_S differs with Q_F used. If Q_F is assumed to be 0 W m^{-2}, SUEWS generally performs well in winter, spring and autumn with *RMSE* 51, 91 and 94 W m^{-2}, respectively (Fig. 5, Table 3). The R^2 is above 0.7 both in winter and spring but considerably lower (0.45) in autumn. Although the shape of the diurnal pattern including sign transition are well replicated, the nocturnal ΔQ_S is slightly underestimated. In summer, ΔQ_S is substantially overestimated during the daytime and underestimated at night (absolute values). When Q_F is included, a large portion goes into the storage heat flux. There is a large improvement in summertime *RMSE* (39 W m^{-2} decrease, Table 3) and smaller in spring and autumn (9 and 14 W m^{-2} decreases, respectively). However, wintertime *RMSE* deteriorates (+26 W m^{-2}). The coefficients of determination have substantial increases for all seasons (0.09, 0.07, 0.19 and 0.18 increases, respectively). From the above analysis, it appears the simulated wintertime Q_F may have greater uncertainty than other seasons.

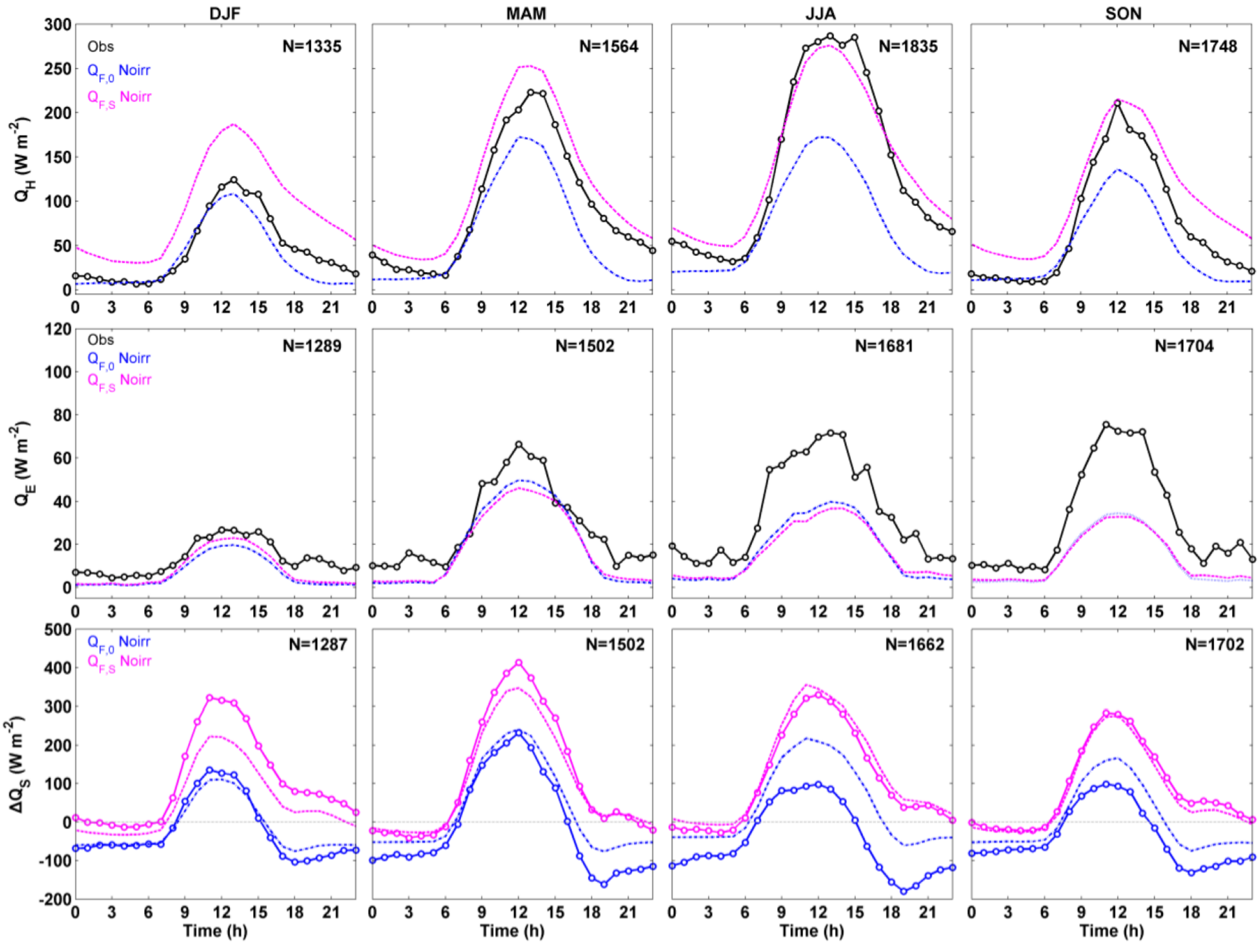

Figure 5: Seasonal mean diurnal cycles of observed and simulated sensible heat flux (Q_H), latent heat flux (Q_E) and storage heat flux (ΔQ_S) for the two experiments ($Q_{F,0}$ *Noirr*, $Q_{F,S}$ *Noirr*). See Table 3 for statistical performance metrics and Figures C.1, C.2, C.3 for scatter plots.

3.3 Latent heat flux

The underestimation of Q_E, especially in summer and autumn, is explored by considering the surface resistance r_s (or its reciprocal, surface conductance g_s) as evapotranspiration is very sensitive to it. The overall capability of water to be transported through the surface (soil, leaves etc) to the lower atmosphere is captured by g_s. The Jarvis-Stewart model (Jarvis, 1976; Stewart, 1988), which has been used extensively in previous studies (e.g. Grimmond and Oke 1991; Ogink-Hendriks, 1995; Matsumoto et al. 2008; Järvi et al. 2011; Ward et al. 2016), is employed in SUEWS to estimate g_s. The response of stomata opening and closing, and other surface controls are included as a synergistic function of the leaf area index (*LAI*), incoming solar radiation ($K\downarrow$), specific humidity deficit (Δq), air temperature (T_a) and soil moisture deficit ($\Delta\theta$):

$$g_s = G_1 g(LAI) g(K\downarrow) g(\Delta q) g(Ta) g(\Delta\theta) \quad (8)$$

Although the specific mathematical formulations of each sub-function may differ among studies, the general form is similar. The five sub-functions are presumed to be independent from each other. Although Δq and T_a are usually highly correlated, some studies found that incorporating both functions provides better results (e.g. Khatun et al. (2011) east Asian forests). Moreover, the shapes of the g_s dependence curves to Δq and T_a are very different (Ward et al. 2016). Low T_a often coincides with low Δq, while low T_a constrains g_s but low Δq favours g_s. The sub-functions range from 0-1, to reduce the maximum surface conductance, except for *g(LAI)*:

$$g(LAI) = \sum_{iv}\left(f_{iv}\, g_{max,iv} \frac{LAI_{iv}}{LAI_{max,iv}}\right) \quad (9)$$

where for the three vegetation types (evergreen, deciduous, grass) *iv* the fraction of area f_{iv}, maximum conductance $g_{max,iv}$, and the maximum *LAI* ($LAI_{max,iv}$) are needed. It should be noted $g_{max,iv}$ is usually larger for irrigated than unirrigated vegetation. For radiative control, the observed maximum incoming solar radiation $K_{\downarrow max}$ is used (here, set to 1200 W m^{-2})

$$g(K\downarrow) = \frac{K\downarrow/(G_2+K\downarrow)}{K\downarrow max/(G_2+K\downarrow max)} \quad (10)$$

where G_2 and other coefficients (G_1-G_6) are obtained from observations (Grimmond and Oke 1991; Ward et al. 2016). For humidity:

$$g(\Delta q) = G_3 + (1-G_3)G_4^{\Delta q} \quad (11)$$

For air temperature, lower T_L and upper T_H temperature limits are used when evaporation turns off ($g(T_a)=0$). Here T_L and T_H are set to a relatively wide range as -10°C and 55°C, respectively.

$$g(Ta) = \frac{(T_a-T_L)(T_H-T_a)^{Tc}}{(G_5-T_L)(T_H-G_5)^{Tc}} \quad (12)$$

with $T_c = \frac{(T_H-G_5)}{(G_5-T_L)}$.

The normalized form of $g(\Delta\theta)$ enables $g(\Delta\theta)=1$ when there is no soil moisture deficit and $g(\Delta\theta)=0$ when the soil moisture deficit equals to the wilting point ($\Delta\theta_{wp}$, here set to 120 mm):

$$g(\Delta\theta) = \frac{1-exp(G_6(\Delta\theta-\Delta\theta_{wp}))}{1-exp(-G_6\Delta\theta_{wp})} \quad (13)$$

The hourly time series for the whole year of each subcomponent of g_s (Eq. 9-13) and for g_s itself (Eq. 8) without irrigation are shown in Figures 6 and 7. In July and August, modelled g_s is smaller (< 1 mm s^{-1}) than other months, explaining the underestimation of Q_E. As $g_s(K\downarrow)$, $g_s(T_a)$ and $g_s(\Delta\theta)$ all have relatively high values from July to September, $K\downarrow$, T_a and $\Delta\theta$ are not key factors for the underestimation of Q_E. July and August 2013 $g_s(\Delta q)$ values are quite small as there are very large specific humidity deficits, associated with the unusually hot and dry conditions (Ao et al. 2016a). Despite this the observed Q_E in these months remained relatively large, probably maintained by irrigation (section 3.4).

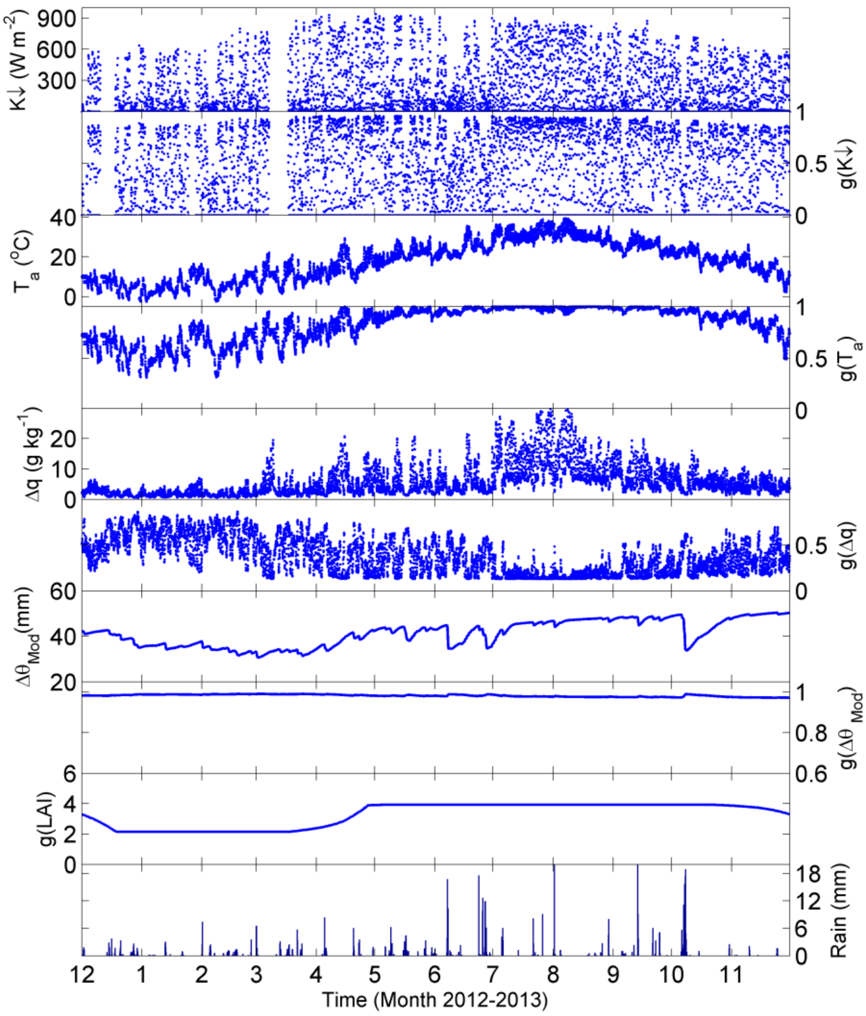

Figure 6: Hourly time series of surface conductance related environmental variables and corresponding sub-components (eqn 10-14). Irrigation is not considered here

3.4 Irrigation

3.4.1 Irrigation scheme evaluation

In Shanghai, it is not easy to obtain accurate external water use data. From field observations, including direct conversations with those undertaking irrigation, and a literature review the behaviours are characterized. At the Shanghai Meteorological Service (150 m radius of site) irrigation is conducted throughout the year on any day of the week. It occurs most intensively in July and August when it is hot. Generally only grass is irrigated. The mostly manual irrigation, usually occurs twice on hot summer days (06:00 to 11:00; 15:00 to 19:00) in different areas so by the end of the day the whole area is irrigated. In winter irrigation occurs once per day (morning or evening) every 3-4 days. Street cleaning and park irrigation are sometimes observed. Irrigation of private gardens may be extremely variable (Mitchell et al. 2001). Based on this, a diurnal profile is assumed. The modelled latent heat flux using this field based diurnal profile when compared with an ideal evenly distributed one show small differences (not shown). f_{grass} and f_{aut} are set to 0.4 and 0, respectively. For $b_{0,m}$, $b_{1,m}$, $b_{2,m}$ the same values as Järvi et al. (2011) are used (Table 2), which are based on Vancouver (Grimmond and Oke 1986; Grimmond and Oke 1991). The water from these are assumed to be included in the coefficients used as no additional detailed information is available.

Previous studies show that evaporation is very sensitive to both the amount and frequency of irrigation (Grimmond and Oke 1986, Vahmani and Hogue 2014). To test the influence of irrigation frequency on Q_E the following scenarios are tested: (i) SUEWS irrigation (Eq. 3) is used with parameter that set irrigation to 0 within 6 hours of rain and with the other parameters as specified in Table 3 (hereafter $Q_{F,S}$ *Irr*); and (ii) as (i) but with irrigation every 3 days independent of weather conditions (Table 3, hereafter $Q_{F,S}$ *Irr 3dGap*).

The monthly water use data from January 2013 to December 2013 for the entire Shanghai (Chang et al. 2015) provided by the Shanghai Water Authority (http://www.shanghaiwater.gov.cn/) are used to evaluate the SUEWS irrigation scheme. As December 2012 water use data are unavailable, December 2013 data are used. The water use data are split between indoor and outdoor assuming the minimum month value is the indoor water use (minimum month method, Vahmani and Hogue 2014). Differences from this minimum are considered to be outdoor water use, and indicative of irrigation and/or street cleaning etc. Uncertainties arise from using city level data given land use and land cover variations around this large city. Total city water use distributed to the Xuhui district (area: 54.76km^2) where the study site is located is based on the annual water use fraction. Further, it is assumed that irrigation is applied to all vegetation and half the road (street cleaning) areas. The annual water use fraction, vegetation and road cover fractions for the Xuhui district are 0.017, 0.232 and 0.522, respectively (Shanghai Municipal Statistics Bureau 2016). The modeled monthly cumulative results from the irrigation scenarios are evaluated against the estimated outdoor water use (Fig. 8). The peak outdoor water use months occurred in July and August (around 18.5 mm month^{-1}), with annual total (97 mm year) corresponds to 9% of the annual rainfall amount. The monthly trend for the *Irr 3dGap* scenario matches the outdoor water use estimates relatively well, with a bit larger annual irrigation amount (140 mm). However, the scenario with only a 6 h gap after rain (*Irr*) results in much larger irrigation rates than suggested from the city outdoor water use (Figure 8). Therefore, the *Irr 3dGap* scenario is considered more appropriate for the study area.

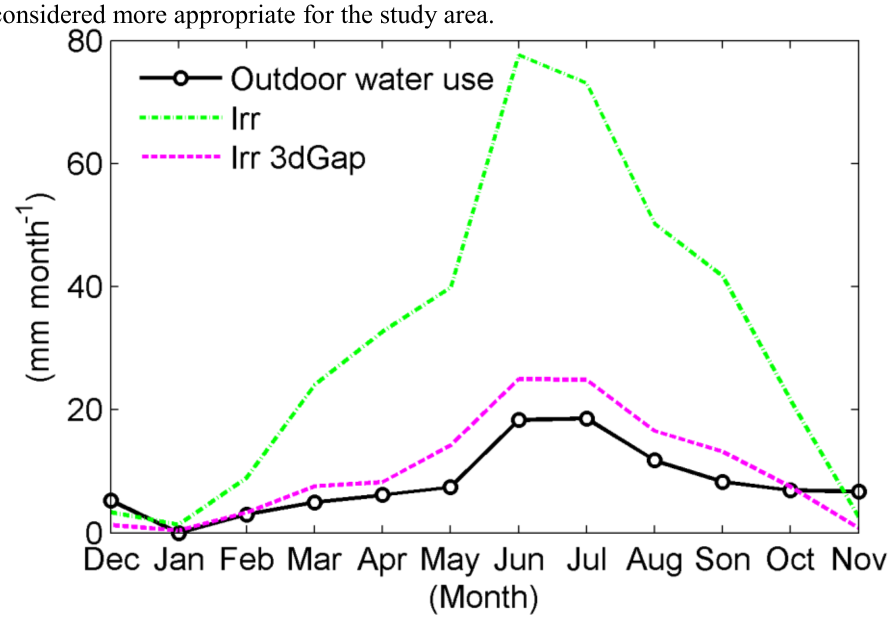

Figure 8: Monthly outdoor water use observed for the area (section 3.4.1) and simulated irrigation.

3.4.2 Impact of Irrigation on simulated surface energy fluxes

For the first irrigation scenario ($Q_{F,S}$ *Irr*) (Figures 9 and C.1), the modelled Q_E have small differences compared to Exp. $Q_{F,S}$ *Noirr* in winter (ΔRMSE -0.3 W m^{-2}, ΔMBE -1.6 W m^{-2}) and spring Q_E (ΔRMSE +0.8 W m^{-2}, ΔMBE -5.8 W m^{-2}) (Table 3). The summer Q_E increased the RMSE (+4.5 W m^{-2}) while the R^2 improved (0.08 to 0.15) and MBE changed sign (negative to positive) (Table 3). The seasonal mean diurnal cycle shows that the daytime summer Q_E is largely overestimated under this irrigation condition (Fig. 9). Irrigation has a very positive impact on modelled Q_E in autumn (ΔRMSE -7.7 W m^{-2}, ΔR^2 +0.14). Sensitivity test of the coefficients $b_{1,m}$ and $b_{2,m}$ (changing from 3 and 1.1 to 2 and 2) amplifies the relative importance of the days after rain, causing a slight decrease in RMSE (not shown).

The trade-off between Q_H and Q_E is obvious as an overestimation of Q_E in summer leads to an underestimation of Q_H (Fig. 9). The summer and autumn Q_H have an increase in RMSE (+22.7 and +0.5 W m^{-2}, respectively), but slight decrease in the other two seasons. The modeled total Q_H and Q_E remain constant between *Noirr* and *Irr* case. As the options selected for ΔQ_S coefficients do not change with soil moisture, irrigation also has no impact on modeled ΔQ_S (not shown).

As the second irrigation scenario ($Q_{F,S}$ *Irr 3dGap*) is less frequent than when irrigation is permitted almost every day except in winter (Fig. 7), the latter annual total irrigation of about 380 mm (~30% of annual rainfall) much larger than the former (~140 mm).

From the seasonal mean diurnal cycles of observed and simulated latent heat flux (Fig. 9), the extreme overestimation of Q_E under the first irrigation scenario in summer is largely improved. Although the diurnal peak is still overestimated with 3-day frequency. The modelled seasonal mean diurnal curves in autumn and spring agree well with the observed curves. The modelled wintertime Q_E change little as there is only a small amount of irrigation. The Q_E RMSE has the largest decrease in summer (-7.7 W m^{-2}). The Q_H RMSE in spring, summer and autumn also decreased (-0.3, -12.1 and -1.5 W m^{-2}) for the second scenario, but increases slightly (< 1 W m^{-2}) in winter.

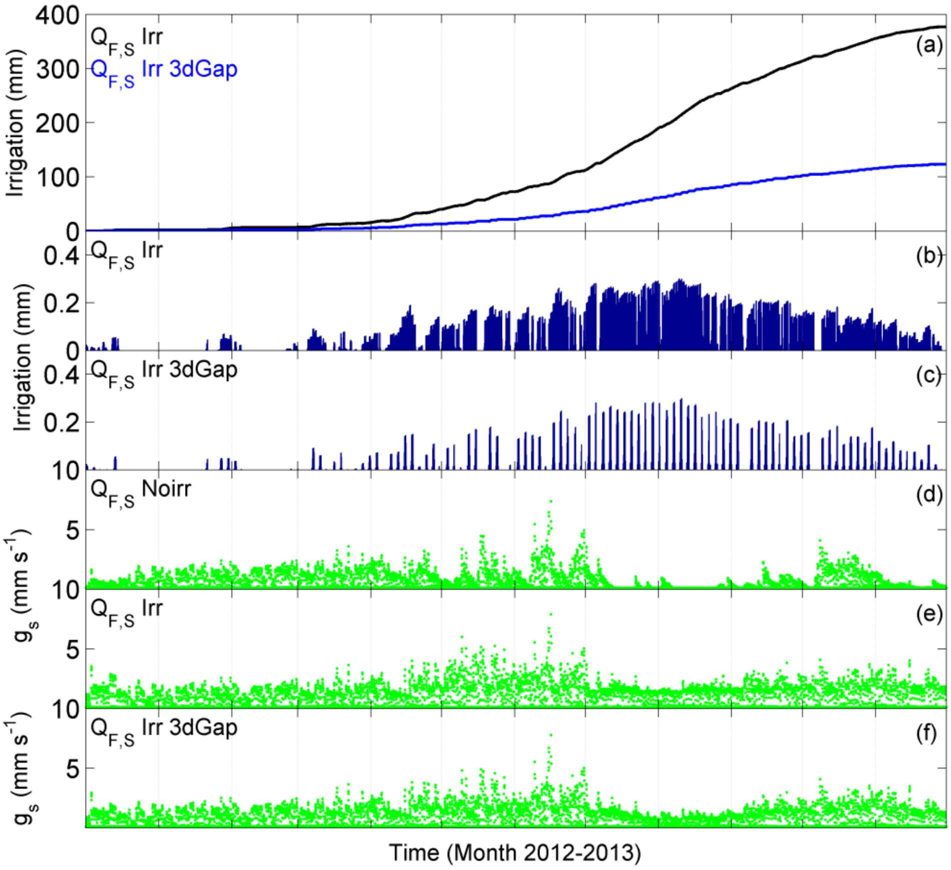

Figure 7: Variation in irrigation (a) cumulative annual total for two scenarios; timing of irrigation for experiment (b) $Q_{F,S}$ *Irr*, and (c) $Q_{F,S}$ *Irr 3dGap*; and hourly modelled surface conductance (g_s) for three scenarios: (d) $Q_{F,S}$ *Noirr,* (e) $Q_{F,S}$ *Irr,* and (f) $Q_{F,S}$ *Irr 3dGap*.

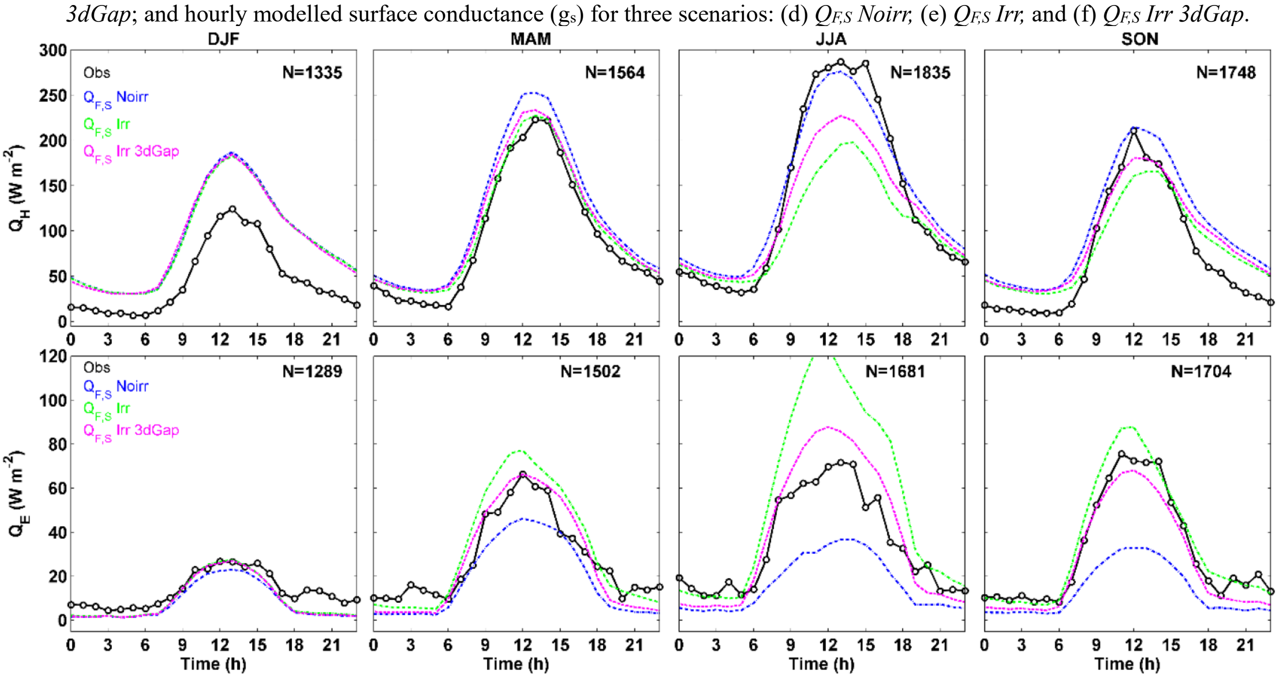

Figure 9: Seasonal mean diurnal cycles of observed and simulated sensible heat flux (Q_H), latent heat flux (Q_E) for three irrigation scenarios (defined in 3.4.1): $Q_{F,S}$ *Noirr*, $Q_{F,S}$ *Irr* and $Q_{F,S}$ *Irr 3dGap*; See Figure C.1 and C.2 for scatterplots.

3.5 Comparison of surface conductance (g_s) among scenarios

With irrigation turned on, the surface conductance has a substantial increase in July, August, September and November (Figures 7d-f). These four months have the least rainfall in summer and autumn (Ao et al. 2016a). When irrigation is reduced to every 3 days, the surface conductance in these months still has an obvious increase compared to the no irrigation scenario, but less than the more frequent irrigation scenario.

Fig. 10a shows the monthly median diurnal cycles of g_s for different scenarios with the observed g_s calculated from the Penman–Monteith equation (Monteith, 1965) with observations:

$$g_s^{-1} = r_s = \left(\frac{s\beta}{\gamma} - 1\right) g_a^{-1} + \frac{\rho c_p VPD}{\gamma Q_E} \qquad (14)$$

where β is the Bowen ratio ($\beta = Q_H/Q_E$), s is the slope of the saturation vapour pressure curve ($P_a\ {}^oC^{-1}$) and is a function of the air temperature, γ is the psychrometer constant ($P_a\ {}^oC^{-1}$) and is determined by air pressure, temperature and humidity, ρ is the density of air, c_p is the specific heat of air at constant pressure, VPD is the vapor pressure deficit which is a function of the air temperature and relative humidity, and g_a is the aerodynamic conductance which describes rate of water transport from the air above leaves to the atmosphere at a certain reference height. g_a is calculated assuming a logarithmic wind profile and therefore is primarily influenced by the wind speed, atmospheric stability and roughness length for momentum (and the boundary layer resistance is impacted by the roughness length for heat).

Similar to central London (Ward et al. 2016), the diurnal cycle of the observed g_s at XJH fluctuates with variable patterns. The monthly median diurnal maximum g_s is around 2-4 mm s^{-1}. The relatively large g_s (both day- and night-time) in winter months is somewhat unexpected. This may be caused by the wet winter with still active grass cover and street cleaning activities. The monthly median diurnal aerodynamic conductance (g_a) is regularly sinusoidal in shape with relatively small monthly variations between scenarios. The monthly median g_a is much larger than g_s (around 12-25 mm s^{-1}), indicating that evaporation is limited by g_s rather than g_a.

The modelled g_s are very different between scenarios. Without irrigation ($Q_{F,S}$ *Noirr*), the g_s is totally constrained (near 0 mm s^{-1}) in July and August. The modelled g_s is consistent with observed g_s in May, June and October, but largely underestimated in winter months. The modelled nocturnal g_s is forced to a constant of 0.1 mm s^{-1}, which is underestimated through the year. When irrigation is supplied continuously ($Q_{F,S}$ *Irr*), the modelled g_s has a substantial increase from May to December and is overestimated during daytime in July and August which causes the overestimation of Q_E in summer. When the irrigation frequency is decreased to every 3 days ($Q_{F,S}$ *Irr 3dGap*), the overestimation of g_s is improved. The modelled g_s during January-April is almost unimpacted by the three scenarios as the irrigation amount is very tiny during this period.

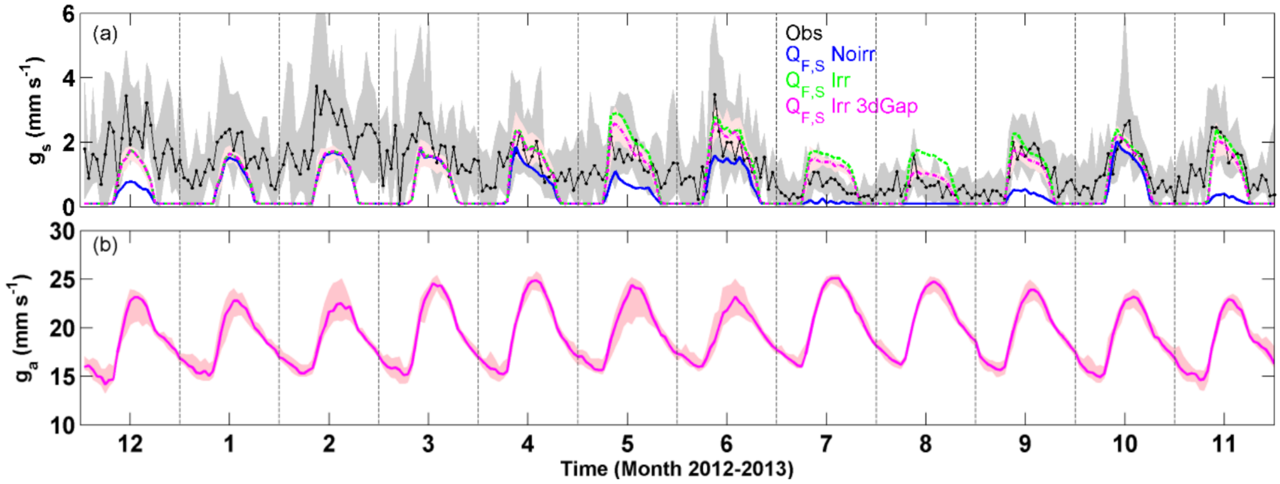

Figure 10: Monthly median diurnal variation with inter-quartile range (shading) of (a) observed (black) and modelled (colour) surface conductance g_s and (b) modelled aerodynamic conductance (g_a) .

4. Discussion and Conclusions

The performance of the urban land surface model SUEWS driven by 1-year of field measurements is evaluated at a central urban site (XJH) in Shanghai focusing on the estimation and impact of the anthropogenic heat flux (Q_F) and irrigation on the surface energy flux components.

SUEWS estimates Q_F as a function of heating and cooling degree days and scheme coefficients are fitted by results from the inventory based LQF model. As such, Q_F estimates from SUEWS are almost the same as LQF. LQF estimates building Q_{FB}, vehicle Q_{FV} and metabolism Q_{FM} components based on city level hourly electricity consumption data, air temperature and population density. A new building heat emission / air temperature response function using two balance points made the seasonal variation of the building Q_{FB} more distinct.

The diurnal patterns of Q_{FB} for weekday, weekend and holidays derived using local electricity data are similar with a peak around 11:00. On holidays there is a larger evening peak around 19:00. Weekday diurnal profile of Q_{FV} derived from local traffic data has two peaks associated with rush hours. The morning peak is more distinct (at 08:00 in all seasons) than the evening peak (at 17:00). Weekends have no distinct peaks. The largest Q_F (estimated by LQF) is in summer with seasonal mean daily peak around 236 W m^2. Winter and autumn have similar mean daily peaks (~190 W m^{-2}) and spring is the smallest (~180 W m^{-2}). Building heat emission is the largest sub-component (~95% of the total Q_F).

The impact of Q_F on surface energy fluxes is explored with (SUEWS, $Q_{F,S}$) and without Q_F ($Q_{F,0}$). Ignoring Q_F, the seasonal diurnal pattern of sensible heat flux (Q_H) is reproduced well generally, but the magnitude of Q_H is underestimated for all seasons. When $Q_{F,S}$ is used, the seasonal mean diurnal Q_H is overestimated throughout the day in winter, spring and autumn. In summer, day- (night-) time Q_H is slightly under (over-) estimated. Overall performance for Q_H is improved in spring, summer and autumn (*RMSE* decreased) but not in winter. For $Q_{F,0}$, SUEWS summer day(night)time storage heat flux (ΔQ_S) is over (under)estimated whereas $Q_{F,S}$ is improved (*RMSE* decreases by 39 W m^{-2}). Spring and autumn have improvements (RMSE decreases of 9 and 14 W m^{-2}, respectively). But winter does not (RMSE increase of 26 W m^{-2}). This indicates winter Q_F may be overestimated.

Underestimation of Q_E is associated with underestimation of the surface conductance (g_s) in summer, mainly caused by large specific humidity deficits. External water supply may maintain evaporation rates. Having the appropriate seasonal cycle of the leaf area index (*LAI*) in winter and spring improve the Q_E model performance. Irrigation amount and frequency have a large impact on Q_E. Seasonal mean summer daytime Q_E is largely overestimated if continuous irrigation is permitted indicating an overestimation of irrigation. In autumn irrigation improves Q_E (RMSE decreased, R^2 increased). Overestimation of Q_E with too frequent irrigation in summer is improved when reduced to every 3 days (RMSE decreased), and slightly improved in spring. Reducing irrigation frequency to 3 days also improves summer Q_H (RMSE decreased).

This study emphasizes the importance of appropriately estimating the anthropogenic heat flux and external water use in dry and hot seasons in urban land surface models. Previous studies have evaluated SUEWS at two sites (urban and suburban) in the same/nearby city with contrasting surface characteristics (Karsisto et al. 2016; Ward et al. 2016). Results suggest that the surface cover, especially the vegetated versus impervious proportion along with the anthropogenic heat emission have the largest impact factors on model performances. The magnitude of Q_F may be substantially smaller at suburban sites because of much lower population densities. The difference of building heights at urban and suburban sites will also influence where Q_F is released into the atmosphere. Larger vegetated fractions in suburban areas may also have more intensive irrigation. Therefore future work is inevitably needed to compare simulation results of this central urban site with suburban sites in Shanghai to improve understanding of potential sources of model biases.

Future SUEWS evaluation should considering seasonal variability in the OHM coefficients for the simulation of the storage heat flux (ΔQ_S). Ward et al. (2016) found adjusting the OHM coefficients for a specific site can significantly improve model performance both for ΔQ_S and therefore other terms most notably Q_H as the residual term. Seasonal variations of surface properties such as albedo, Bowen ratio, wind speed and soil moisture (Arnfield and Grimmond 1998, Sun et al. 2017) have critical impacts on ΔQ_S. Adjusting OHM coefficients should analyze more observations and use the recently developed AnOHM (Sun et al. 2017) to determine a wider range of parameters.

Acknowledgements
This work was supported by the National Natural Science Foundation of China (Grant No. 41775019, 41675008), Newton Fund/Met Office Climate Science for Service Partnership (CSSP) China (SG), the Project of Science and Technology Commission of Shanghai Municipality (Grant No. 17DZ1205300), the Project of Scientific and Technological Development of the Shanghai Meteorological Service (Grant No. MS201803) and the fund from China Scholarship Council (CSC). We thank everyone who contributed to instrument maintenance, data collection and model development.

Appendix A: Anthropogenic Heat Flux

LQF (Gabey et al. 2018) is a new implementation of the Large scale Urban Consumption of energY model (LUCY, Allen et al. 2011, Lindberg et al. 2013). LQF or **L**UCY **QF** is embedded in UMEP (Urban Multi-scale Environmental Predictor), which is an open-source city-based climate service tool that combines models and tools for climate simulations (Lindberg et al. 2018). LQF takes a 'top-down' approach using publicly available annual energy consumption data for a large area (e.g. country, province, city) with high resolution population density data to distribute the energy consumption across the area of interest. It separately considers three emission sources: buildings Q_{FB}, traffic Q_{FV} and metabolism Q_{FM} (Grimmond 1992, Sailor 2011). Like the SUEWS method, the daily totals are a function of temperatures (temperature response function) and sub-daily patterns are based on diurnal use profiles.

A.1 LQF temperature response function

Variations of energy consumption with air temperature can be modelled with a single balance point temperature T_b (Eq. (2)) obtained from when the energy consumption is lowest. Consequently, T_b varies with climate (Amato et al. 2005) and/or with building type. Therefore, it is preferable to have the appropriate local T_b as it has a large impact on seasonal variations of the building anthropogenic heat emissions. This approach is used in $Q_{F,S}$ (SUEWS) and was originally used in LQF ($Q_{F,L}$). In this work we introduced a new LQF temperature response function (Fig. 2) with two balance point temperatures, i.e. threshold temperatures when heating (T_h) and cooling (T_c) commence.

To quantify T_b for Shanghai, the whole city electricity consumption (Liu and Cao 2013) and XJH air temperature data are analyzed (Fig. 2b). Ideally all sources of energy would be analysed, but electricity consumption data are often used as a proxy for building heat release. For example, Kikegawa et al. (2014) estimate that in Tokyo ~80% of office building energy demand in summer is from electricity consumption. The buildings in the XJH area are predominately office and residential buildings, with very little industry. Shanghai Municipal Statistics Bureau (2016) indicates industry around the dense urban XJH site (f_{inu}) accounts for about 10% of total energy consumption. In contrast, suburban districts such as Jiading has a much higher industry fraction.

Given the similar climatic regime, building energy consumption at our study site is assumed to be like Tokyo. However, Shanghai's electricity consumption is only 14% of the total energy consumption (Table 1). As industry consumption is relatively insensitive to weather conditions (Sailor 2011), it has a different profile to the commercial study site of interest, with reduced daily amplitude and seasonal variations. Given the difficulty of accessing details of industrial consumption patterns, for simplicity the industrial load is assumed to be uniform through the day (Sailor 2011).

The relation between energy consumption and air temperature is analyzed. In Shanghai, the energy consumption rises almost linearly when the daily mean air temperature is warmer than 21°C or cooler than 15°C, providing evidence that cooling or heating systems are operating in these temperature ranges (Fig. 2b). In the "comfortable" range (15 to 21°C) energy consumption stays nearly constant. The energy consumption for cooling increases more rapidly than for heating as central heating system are absent south of an east-west ('Qin-Huai') line near 33 °N (Makinen 2014, Shi et al. 2016). Given this in SUEWS, a single T_b of 20 °C is used.

In LQF the three components of Q_F (building, transport, metabolism) are treated separately. A temperature response function (f_b) modifies the base daily building energy consumption $E_{B,b}$ (kWh d^{-1} capita^{-1}).

$$Q_{F,b\ L,daily} = \rho_{pop} \bullet f_b \bullet E_{B,b} \qquad \text{(A.1)}$$

where ρ_{pop} is the population density of XJH site (N_{pop} = 261.62 capita ha^{-1}). Here the original LQF one balance point temperature function (Allen et al. 2011, Lindberg et al. 2013, Fig. 2b, dotted line) is modified to allow minimum energy consumption to occur over a range of temperatures. Threshold temperatures when heating (T_h) and cooling (T_c) commence, and when saturation energy use occurs as additional energy consumption is minimal (Fig. 2a, solid line); i.e. < T_{min} no additional heating occurs (> T_{max} for cooling). Therefore, logic variables (l_{c1}, l_{h1}) are 0 except when the air temperature is with a critical range (Fig. 2b):

$$T_{max} > T_a > T_c \qquad l_{c1} = 1;$$
$$T_{min} < T_a < T_h \qquad l_{h1} = 1$$

to allow:

$$f_b = b_b + A_c\,|T_a - T_c|\,l_{c1} + A_h\,|T_a - T_h|\,l_{h1} \qquad \text{(A.2)}$$

Or more completely:

$$f_b = b_b + A_c\,|T_a - T_c|\,l_{c1} + A_h\,|T_a - T_h|\,l_{h1} + l_{h2}\,b_h + l_{c2}\,b_c$$

with two logic variables (l_{c2}, l_{h2}) which are non-zero when:

$$T_a \geq T_{max}\ \ l_{c2} = 1 \ \text{or}\ T_a \leq T_{min} \qquad l_{h2} = 1.$$

The three non-dimensional coefficients b_b, b_c and b_h are the base fraction of energy use when small changes in daily air temperature have no impact. The comfortable air temperature range (i.e. between T_h and T_c) for b_b and then once all heating (b_h) or cooling (b_c) are on. A_c and A_h are the building energy consumption thermal response slopes for cooling (heating) when daily air temperature warmer (colder) than T_c (T_h).

To determine the parameter values for Shanghai the 2005 to 2009 city wide electricity consumption data (Liu and Cao 2013) are used (Fig. 2b). The resulting parameters are b_b=0.88, A_c=0.04 °C^{-1}, and A_h=0.01 °C^{-1}. In this subtropical city, the larger cooling coefficient A_c reflects the absence of a centralized heating system in Shanghai, but extensive use of air conditioning in summer.

A.2 Vehicle based heat emissions

The heat released by motor vehicles (Q_{FV}) from combustion of petrol or diesel fuel (Sailor 2011) generally does not have seasonal variations (Sailor and Lu, 2004). In LQF, Q_{FV} is calculated as a function of vehicle numbers (cars 89, motorcycles 17.2, freight vehicles 8.8 per 1000 capita; Shanghai Municipal Statistics Bureau 2016), traffic speed, and time (days, hour). The fuel type is assumed to be petrol (Zhao 2007). The mean vehicle speed is set to 48 km h^{-1} (Su et al. 2014).

Hourly highway traffic data (traffic count and speed) for the inner ring of Shanghai in 2011 are used to derive the diurnal profiles for weekdays, weekends and holidays (Fig. 3b). These are applied to all roads in the study area (see section 3.1).

A.3 Population density

In LQF, the default population is from the Gridded Population of the World, Version 4 (GPWv4, CIESIN, 2010) with estimates for 2005, 2010 and 2015. The 2010 30 arc-second (~1 km) population density around the XJH site is about 261.62 capita ha^{-1} (GPWv4, CIESIN, 2010) whereas the statistics in 2013 (Shanghai Municipal Statistics Bureau of Xuhui District 2013) for the XJH site neighbourhood (4.07 km^2) has a permanent resident population of 92,764 (i.e. 227.92 capita ha^{-1}). Here the population density of 261.62 capita ha^{-1} is used as the resolution is closer to the source area of XJH site.

Urban population density varies significantly through the course of a day and from working days to non-working days (Gabey et al. 2018), particularly in areas such as XJH with a mix of permanent residents, shoppers, tourists, hospital visitors and patients, *etc.* who come and go. The publicly available data from the national census of Shanghai do not capture these dynamics. Yu and Wen (2016) estimate day- and night-time population for the Jing'an district using land use and population age structure data. They suggest the daytime population is 39.2% higher than at night for the district as a whole (and 147.7% higher in the busiest sub-district). Zhong et al.'s (2017) analysis of cell phone signals found from 06:00 to 10:00 people move into the centre of Shanghai from outer areas, with a peak at 10:00 that is sustained until 18:00, when the return to suburban areas occurs. The day to night population density ratio in central Shanghai is about 1.5 (Zhong et al.'s 2017 Fig. 7). Based on these two studies, the daytime (10:00 – 18:00) population is assumed to be 1.5 times the nocturnal population at XJH site, with the periods 06:00 – 10:00 and 18:00-22:00 being transition periods when the population moves between work, leisure and residential sites (a linear increase (decrease) is assumed, following Sailor and Lu 2004). Using this dynamic ratio, and assuming the daytime and nocturnal population for the whole Shanghai is roughly conserved, the diurnal variation of the electricity consumption is further scaled.

Appendix B Statistical evaluation techniques

Common statistical metrics are used to assess model performance. The modeled (M_i) and observed (O_i) values, are used with their corresponding mean values ($\bar{M}, \bar{O}$) to calculate the coefficient of determination (R^2):

$$R^2 = \left[\frac{\sum_{i=1}^{N}(M_i-\bar{M})(O_i-\bar{O})}{\sqrt{\sum_{i=1}^{N}(M_i-\bar{M})^2}\sqrt{\sum_{i=1}^{N}(O_i-\bar{O})^2}}\right]^2,$$

the root mean square error (*RMSE*):

$$RMSE = \sqrt{\frac{1}{N}\sum_{i=1}^{N}(M_i - O_i)^2},$$

mean bias error (*MBE*):

$$MBE = \frac{1}{N}\sum_{i=1}^{N}(M_i - O_i)$$

and the mean absolute error (*MAE*):

$$MAE = \frac{1}{N}\sum_{i=1}^{N}|M_i - O_i|$$

The RMSE, MBE and MAE all have units of the variable analysed and ideal value of 0; whereas R^2 varies between 0 and 1 with an ideal value of 1.

Appendix C. Simulated versus observed fluxes

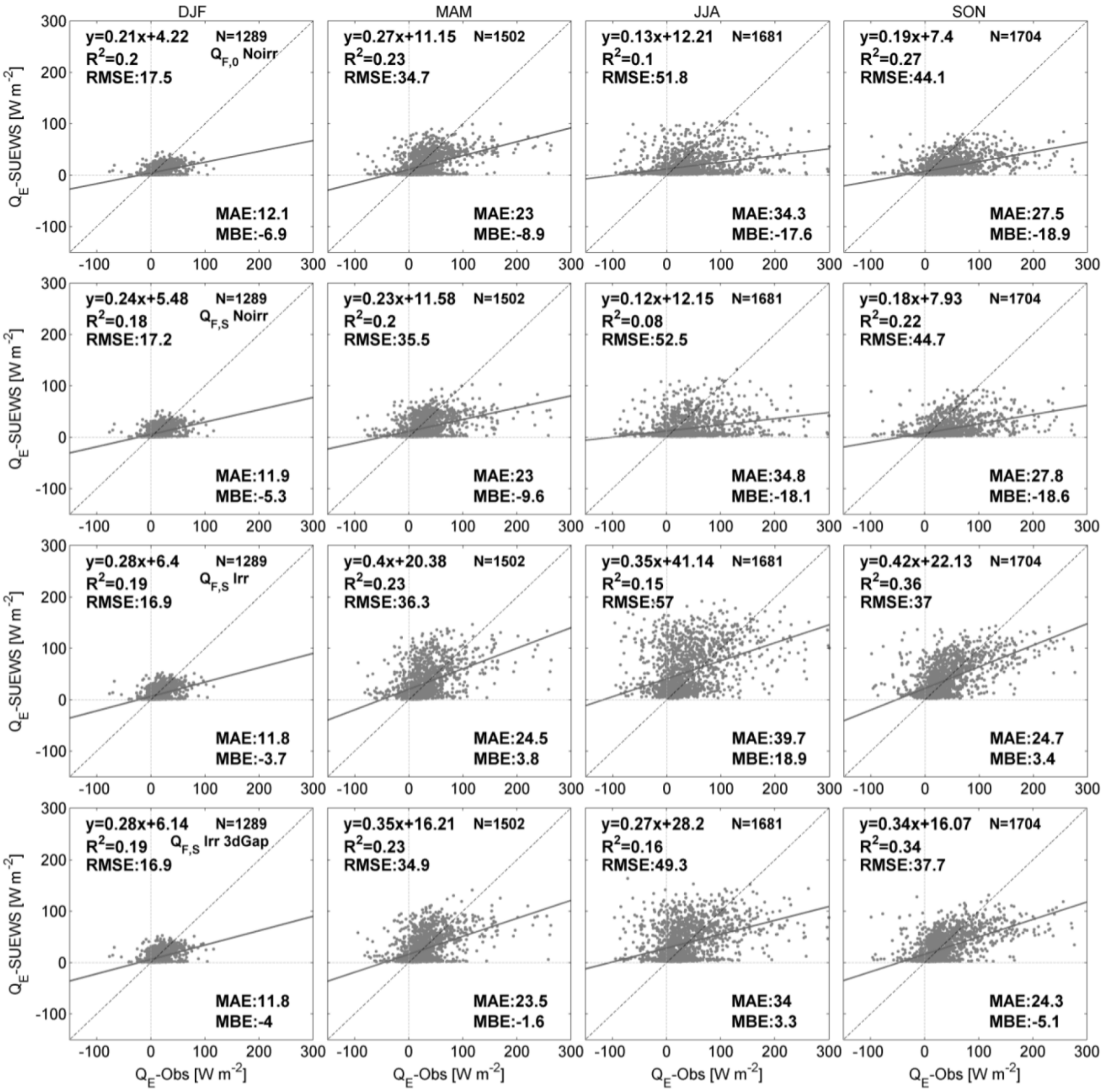

Figure C.1. Simulated versus observed latent heat flux (Q_E) for each experiment ($Q_{F,0}$ *Noirr*, $Q_{F,S}$ *Noirr*, $Q_{F,S}$ *Irr*, $Q_{F,S}$ *Irr 3dGap*,). Statistics shown are coefficient of determination (R^2), root mean square error (RMSE), mean absolute error (MAE) and mean bias error (MBE).

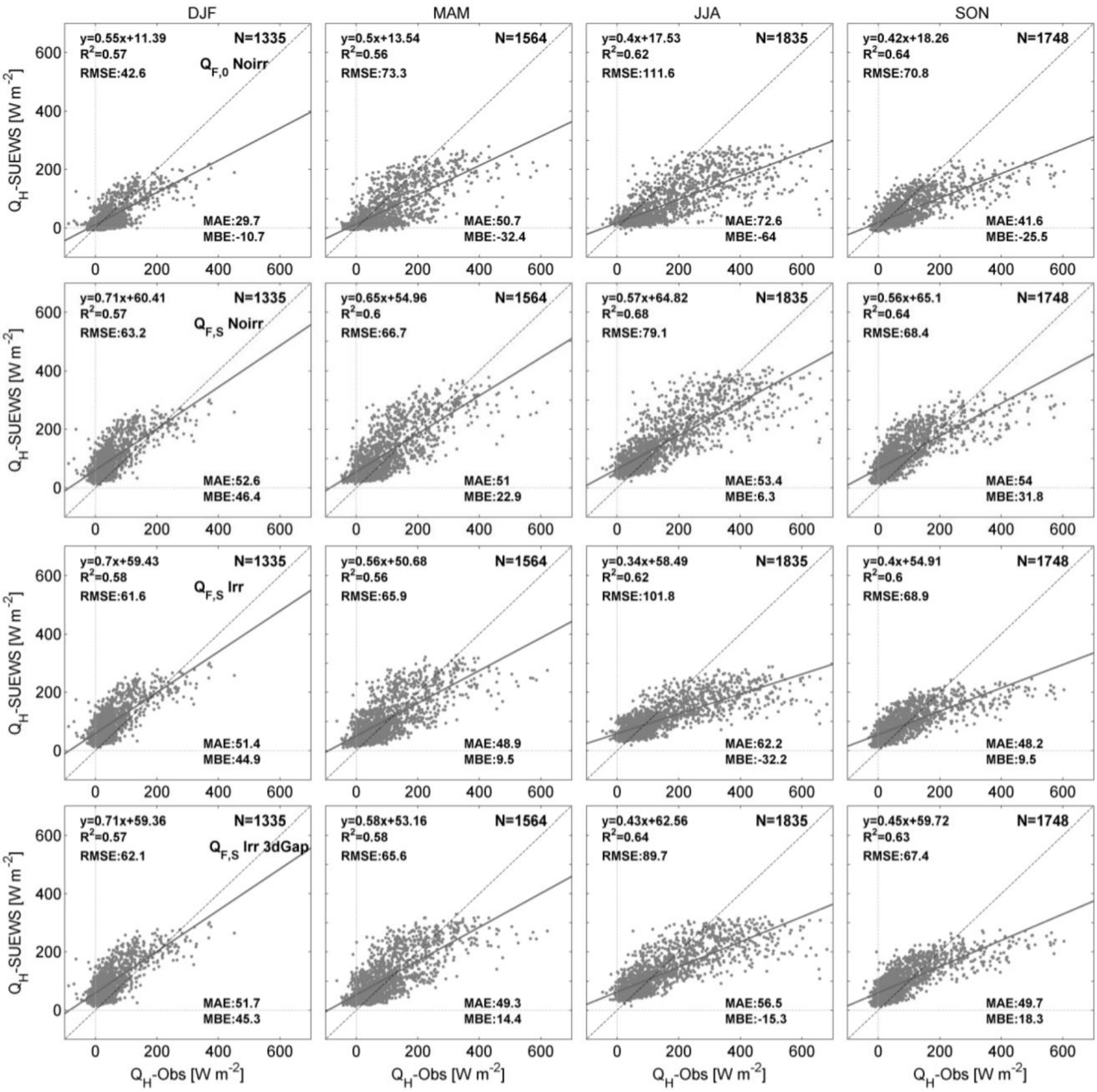

Figure C.2. As Figure C.1., but for sensible heat flux (Q_H).

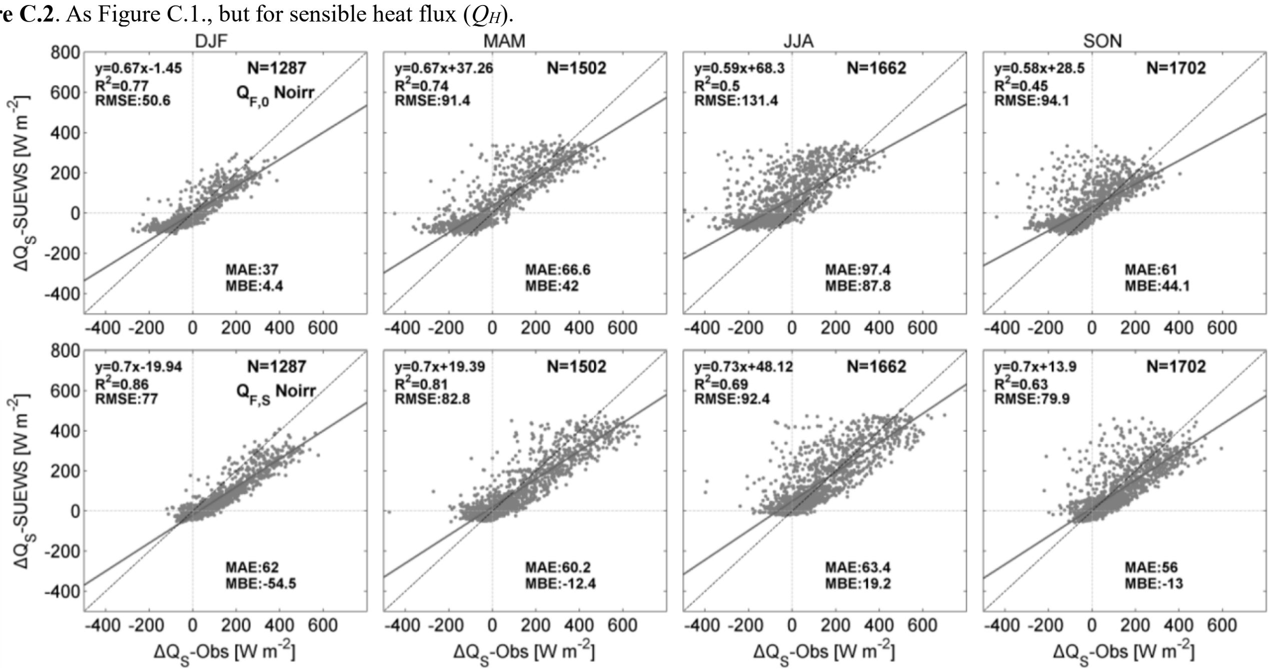

Figure C.3. As Figure C.1, but storage heat flux (ΔQ_S). As OHM coefficients varying with soil moisture are not used, irrigation has no influence on ΔQ_S, the results of related experiments are not shown.

References

Alexander, P. J., G. Mills and R. Fealy, 2015: Using LCZ data to run an urban energy balance model. *Urban Clim.* **13**, 14–37, doi: 10.1016/j.uclim.2015.05.001.

Allen, L., F. Lindberg and C. S. B. Grimmond, 2011: Global to city scale urban anthropogenic heat flux: Model and variability. *Int. J. Climatol.*, **31**, 1990–2005, doi: 10.1002/joc.2210.

Amato, A. D., M. Ruth, P. Kirshen and J. Horwitz, 2005: Regional energy demand responses to climate change: methodology and application to the Commonwealth of Massachusetts. *Climatic Change*, **71**, 175–201.

Anandakumar, K., 1999: A study on the partition of net radiation into heat fluxes on a dry asphalt surface. *Atmos. Environ.*, **33**, 3911–3918.

Ao, X., C. S. B. Grimmond, Y. Chang, D. Liu, Y. Tang, P. Hu, Y. Wang, J. Zou and J. Tan, 2016a: Heat, water and carbon exchanges in the tall megacity of Shanghai: Challenges and results. *Int. J. Climatol.*, **36**, 4608-4624.

Ao, X., C. S. B. Grimmond, D. Liu, Z. Han, P. Hu, Y. Wang, X. Zhen and J. Tan, 2016b: Radiation fluxes in a business district of Shanghai, China. *J. Appl. Meteor. Climatol.,* **55**, 2451-2468.

Arnfield, A.J. and C. S. B. Grimmond, 1998: An urban canyon energy budget model and its application to urban storage heat flux modeling. *Energy Build*, **27**, 61-68.

Asaeda, T. and V. Ca, 1993: The subsurface transport of heat and moisture and its effect on the environment: a numerical model. *Bound.-Layer Meteorol*., **65**, 159–179.

Best, M. J. and C. S. B. Grimmond, 2016a: Investigation of the impact of anthropogenic heat flux within an urban land surface model and PILPS-urban. *Theor. Appl. Climatol.*, **126**, 51-60, doi: 10.1007/s00704-015-1554-3.

Best, M. J. and C. S. B. Grimmond, 2016b: Modelling the partitioning of turbulent fluxes at urban sites with varying vegetation cover. *J. Hydrometeor*., **17**, 2537-2553, doi: 10.1175/JHM-D-15-0126.1.

Chang, Y., J. Tan, J. Peng and W. Gu, 2015: Relativity analysis of daily water supply and meteorology factor and establishment of forecast model in Shanghai (in Chinese). *Journal of Water Resources & Water Engineering,* **26**, 32-36.

Chen, F. and J. Dudhia, 2001: Coupling an Advanced Land Surface–Hydrology Model with the Penn State–NCAR MM5 Modeling System. Part I: Model Implementation and Sensitivity. *Mon. Wea. Rev.*, **129**, 569-585.

Chen, F., and Coauthors, 2011: The integrated WRF/urban modeling system: Development, evaluation, and applications to urban environmental problems. *Int. J. Climatol.*, **31**, 273–288.

Chen, F., X. Yang and J. Wu, 2016a: Simulation of the urban climate in a Chinese megacity with spatially heterogeneous anthropogenic heat data. *J. Geophys. Res. Atmos.*, **121**, 5193-5212.

Chen, L., M. Zhang and Y. Wang, 2016b: Model analysis of urbanization impacts on boundary layer meteorology under hot weather conditions: a case study of Nanjing, China. *Theor. Appl. Climatol.*, **125**, 1-16.

Chow, W. T., F. Salamanca, M. Georgescu, A. Mahalov, J. M. Milne and B. L. Ruddell, 2014: A multi-method and multi-scale approach for estimating city-wide anthropogenic heat fluxes. *Atmos. Environ*., **99**, 64-76.

Christen, A. and R. Vogt, 2004: Energy and radiation balance of a central European city. *Int. J. Climatol.*, **24**, 1395–1421.

CIESIN, Columbia University and Centro Internacional de Agricultura Tropical (CIAT), 2010: Gridded Population of the World Version 3 (GPWv3): Population Density Grids. Palisades, NY: Socioeconomic Data and Applications Center (SEDAC), Columbia University, [Online]. Available from: <http://sedac.ciesin.columbia.edu/gpw>

Coutts, A. M., N. J. Tapper, J. Beringer, M. Loughnan and M. Demuzere, 2013: Watering our cities: the capacity for water sensitive urban design to support urban cooling and improve human thermal comfort in the Australian context. *Prog. Phys. Geogr.*, **37**, 2–28.

Demuzere, M., A. M. Coutts, M. Göhler, A. M. Broadbent, H. Wouters, N. P. M. van Lipzig and L. Gebert, 2014: The implementation of biofiltration systems, rainwater tanks and urban irrigation in a single-layer urban canopy model. *Urban Climate*, **10**, 148-170.

Demuzere, M., S. Harshan, L. Järvi, M. Roth, C. S. B. Grimmond, V. Masson, K. W. Oleson, E. Velasco and H. Wouters, 2017: Impact of urban canopy models and external parameters on the modelled urban energy balance in a tropical city. *Q. J. R. Meteorol. Soc.*, **143**, 1581-1596.

Ding, A., X. Huang, W. Nie, J. Sun, V. M. Kerminen, T. Petäjä, H. Su, Y. Cheng, X. Yang, M. Wang, X. Chi, J. Wang, A. Virkkula, W. Guo, J. Yuan, S. Wang, R. Zhang, Y. Wu, Y. Song, T. Zhu, S. Zilitinkevich, M. Kulmala and C. Fu, 2016: Enhanced haze pollution by black carbon in megacities in China, *Geophys. Res. Lett.*, **43**, 2873-2879.

Doll, D., J. K. S. Ching and J. Kaneshiro, 1985: Parameterization of subsurface heating for soil and concrete using net radiation data. *Bound.-Layer Meteorol*., **32**, 351–372.

Feng, J. M., Y. L. Wang, Z. G. Ma and Y. H. Liu, 2012: Simulating the regional impacts of urbanization and anthropogenic heat release on climate across China. *J. Climate*, **25**, 7187–7203, doi:10.1175/JCLI-D-11-00333.1.

Foken, T., 2008: The energy balance closure problem: an overview. *Ecol. Appl.* 18, 1351-1367.

Fuchs, M., A. Hadas, 1972: The heat flux density in a non-homogeneous bare loessial soil. *Bound.-Layer Meteorol.*, **3**, 191–200.

Gabey A, S. Grimmond and I. Capel-Timms, 2018: Anthropogenic Heat Flux: advisable spatial resolutions when input data are scarce. *Theor. Appl. Climatol*., https://doi.org/10.1007/s00704-018-2367-y

Grimmond C. S. B, M. Blackett, M. J. Best, J. J. Baik, S. E. Belcher, J. Beringer, S. I. Bohnenstengel, I. Calmet, F. Chen, A. Coutts, A. Dandou, K. Fortuniak, M. L. Gouvea, R. Hamdi, M. Hendry, M. Kanda, T. Kawai, Y. Kawamoto, H. Kondo, E. S. Krayenhoff, S. H. Lee, T. Loridan, A. Martilli, V. Masson, S. Miao, K. Oleson, R. Ooka, G. Pigeon, A. Porson, Y. H. Ryu, F. Salamanca, G. J. Steeneveld, M. Tombrou, J. A. Voogt, D. T. Young and N. Zhang, 2011: Initial results from Phase 2 of the international urban energy balance model comparison. *Int. J. Climatol.*, **31**, 244–272.

Grimmond CSB, M Blackett, M Best, J Barlow, JJ Baik, S Belcher, SI Bohnenstengel, I Calmet, F Chen, A Dandou, K Fortuniak, ML Gouvea, R Hamdi, M Hendry, T Kawai, Y Kawamoto, H Kondo, ES Krayenhoff, SH Lee, T Loridan, A Martilli, V Masson, S Miao, K Oleson, G Pigeon, A Porson, YH Ryu, F Salamanca, GJ Steeneveld, M Tombrou, J Voogt, D Young, N Zhang **2010**: The International Urban Energy Balance Models Comparison Project: First results from Phase 1. *J. Appl. Meteorol. Climatol.*, **49**, 1268-92.

Grimmond, C. S. B. and T. R. Oke, 1986: Urban water-balance: 2. Results from a suburb of Vancouver, British-Columbia. *Water Resour. Res.*, **22**, 1404–1412.

Grimmond, C. S. B. and T. R. Oke, 1999: Heat storage in urban areas: Local-scale observations and evaluation of a simple model. *J. Appl. Meteorol. Climatol.*, **38**, 922–940.

Grimmond, C. S. B. and T. R. Oke, 1991: An evaporation-interception model for urban areas. *Water Resour. Res.*, **27**: 1739–1755.

Grimmond, C. S. B., H. A. Cleugh and T. R. Oke, 1991: An objective urban heat storage model and its comparison with other schemes, *Atmos. Environ.*, **25**, 311–326.

Grimmond, C.S.B., 1992: The suburban energy balance: methodological considerations and results for a mid-latitude west coast city under winter and spring conditions. *Int. J. Climatol.*, **12**, 481-497.

Guo, W., X. Wang, J. Sun, A. Ding and J. Zou, 2016: Comparison of land-atmosphere interaction at different surface types in the mid- to lower reaches of the Yangtze river valley. *Atmos. Chem. Phys.*, **16**, 1-42.

Hallenbeck, M., M. Rice, B. Smith, B, C. Cornell-Martinez and J. Wilkinson, 1997: Vehicle Volume Distribution by Classification. Washington

State Transportation Center, p. 54. University of Washington, 1107 NE 45th St. Suite 535, Seattle WA 98105. http://depts.washington.edu/trac.

Ichinose T., K. Shimodozono and K. Hanaki, 1999: Impact of anthropogenic heat on urban climate in Tokyo. *Atmos. Environ.*, **33**, 3897-3909.

Järvi, L., C. S. B. Grimmond and A. Christen, 2011: The surface urban energy and water balance scheme (SUEWS): Evaluation in Los Angeles and Vancouver, *J. Hydrol*., **411**, 219–237.

Järvi, L., C. S. B. Grimmond, M. Taka, A. Nordbo, H. Setälä and I. B. Strachan, 2014: Development of the Surface Urban Energy and Water balance Scheme (SUEWS) for cold climate cities. *Geosci. Model Dev.*, **7**, 1691-1711.

Järvi, L., C. S. B. Grimmond, J. P. Mcfadden, A. Christen, I. B. Strachan, M. Taka, L. Warsta and M. Heimann, 2017: Warming effects on the urban hydrology in cold climate regions. *Scientific Reports*, **7**, 5833.

Jarvis, P. G., 1976: The interpretation of the variations in leaf water potential and stomatal conductance found in canopies in the field. *Philos. Trans. R. Soc. London, Ser. B.*, **273**, 593–610.

Jiang, Y., X. -Q. Yang and X. Liu, 2015: Seasonality in anthropogenic aerosol effects on East Asian climate simulated with CAM5. *J. Geophy. Res. Atmos.*, **120**, 10837–10861.

Kanda, M., A. Inagaki, T. Miyamoto, M. Gryschka and S. Raasch, 2013: A new aerodynamic parametrization for real urban surfaces. *Bound.-Layer Meteorol.*, **148**, 357–377.

Karsisto, P., C. Fortelius, M. Demuzere, C. S. B. Grimmond, K. W. Oleson, R. Kouznetsov, V. Masson and L. Järvi, 2016: Seasonal surface urban energy balance and wintertime stability simulated using three land-surface models in the high-latitude city Helsinki. *Q. J. R. Meteorol. Soc.*, **142**, 401-417, doi: 10.1002/qj.2659.

Kent, C. W., S. Grimmond, J. Barlow, D. Gatey, S. Kotthaus, F. Lindberg and C. H. Halios, 2017: Evaluation of urban local-scale aerodynamic parameters: implications for the vertical profile of wind speed and for source areas. *Bound.-Layer Meteorol.*, **164**, 183–213.

Khatun, R., T. Ohta, A. Kotani, J. Asanuma, M. Gamo, S. Han, T. Hirano, Y. Nakai, N. Saigusa, K. Takagi, H. Wang and N. Yoshifuji, 2011: Spatial variations in evapotranspiration over East Asian forest sites. I. Evapotranspiration and decoupling coefficient. *Hydrological Research Letters*, **5**, 83–87.

Kikegawa, Y., A.Tanaka, Y. Ohashi, T. Ihara and Y. Shigeta, 2014: Observed and simulated sensitivities of summertime urban surface air temperatures to anthropogenic heat in downtown areas of two Japanese Major Cities, Tokyo and Osaka. *Theor. Appl. Climatol.*, **117**, 175–193.

Kljun, N. P., P. Calanca, M. V. Rotach and H. P. Schmid, 2004: A simple parameterisation for flux footprint predictions. *Bound.-Layer Meteorol.*, **112**, 503–523.

Kokkonen, T. V., C. S. B. Grimmond, O. Räty, H. C. Ward, A. Christen, T. R. Oke, S. Kotthaus and L. Järvi, 2018: Sensitivity of Surface Urban Energy and Water Balance Scheme (SUEWS) to downscaling of reanalysis forcing data. *Urban Climate*, **23**, 36-52.

Kotthaus, S. and C. S. B. Grimmond, 2014: Energy exchange in a dense urban environment – Part I: Temporal variability of long-term observations in central London. *Urban Climate*, **10**, 261–280.

Kusaka, H., H. Kondo, Y. Kikegawa and F. Kimura, 2001: A simple singlelayer urban canopy model for atmospheric models: comparison with multi-layer and slab models. *Bound.-Layer Meteorol.*, **101**, 329–358.

Kyle's Converter 2017: Convert Tons Of Coal Equivalent to Kilowatt-Hours. http://www.kylesconverter.com/Energy,-Work,-and-Heat/Tons-of-Coal-Equivalent-to-Kilowatt-Hours (last accessed: 1 December 2017).

Li, D., T. Sun, M. Liu, L. Yang, L. Wang, and Z. Gao, 2015: Contrasting responses of urban and rural surface energy budgets to heat waves explain synergies between urban heat islands and heat waves. *Environ. Res. Lett.*, **10**, 054009, doi:10.1088/1748-9326/10/5/054009.

Lindberg, F., C. S. B. Grimmond, N. Yogeswaran, S. Kotthaus and L. Allen, 2013: Impact of city changes and weather on anthropogenic heat flux in Europe 1995–2015. *Urban Clim.*, **4**, 1–15.

Lindberg, F., C. S.B. Grimmond, A. Gabey, B. Huang, C. W. Kent, T. Sun, N.E. Theeuwes, L. Järvi, H. Ward, I. Capel-Timms, Y. Y. Chang, P. Jonsson, N. Krave, D. W. Liu, D. Meyer, K. F. G. Olofson, J. G. Tan, D. Wästberg, L. Xue and Z. Zhang **2018**: Urban multiscale environmental predictor (UMEP) - An integrated tool for city-based climate services *Environmental Modelling and Software*, **99**, 70–87.

Liu, H. and L. Cao, 2013: The relationship between power load and meteorological factors with refined power load forecast in Shanghai (in Chinese). *Journal of Applied Meteorological Science,* **24**, 455-463.

Loridan, T., C. S. B. Grimmond, B. D. Offerle, D. T. Young, T. E. L. Smith, L. Järvi, F. Lindberg, 2011: Local-scale urban meteorological parameterization scheme (LUMPS): longwave radiation parameterization and seasonality-related developments. *J. Appl. Meteorol. Climatol.*, **50**, 185–202. http://dx.doi.org/10.1175/2010JAMC2474.1.

Loridan, T., F. Lindberg, O. Jorba, S. Kotthaus, S. Grossman-Clarke and C. S. B. Grimmond, 2013: High resolution simulation of surface heat flux variability across central London with Urban Zones for Energy partitioning. *Bound.-Layer Meteorol.*, **147**, 493-523.

Lu, Y., Q. Wang, Y. Zhang, P. Sun and Y. Qian, 2016: An estimate of anthropogenic heat emissions in China. *Int. J. Climatol.*, **36**, 1134-1142.

Makinen, J. 2014: For central heat, China has a north-south divide at Qin-Huai line, Los Angeles Times. http://www.latimes.com/world/asia/la-fg-china-heat-20141115-story.html (last accessed: 15 November 2017)

Masson, V, and Coauthors, 2013: The SURFEXv7.2 land and ocean surface platform for coupled or offline simulation of earth surface variables and fluxes. *Geosci. Model Dev.*, **6**, 929–960.

Matsumoto, K., T. Ohta, T. Nakai, T. Kuwada, K. Daikoku, S. Iida, H. Yabuki, A. V. Kononov, M. K. van der Molen, Y. Kodama, T. C. Maximov, A. J. Dolman and S. Hattori, 2008: Responses of surface conductance to forest environments in the Far East. *Agric. For. Meteorol.*, **148**, 1926–1940, doi: 10.1016/j.agrformet.2008.09.009.

McCaughey, J. H., 1985: Energy balance storage terms in a mature mixed forest at Petawawa, Ontario-a case study. *Bound.-Layer Meteorol.*, **31**, 89–101.

McMaster, G. S. and W. W. Wilhelm, 1997: Growing degree-days: one equation, two interpretations. *Agric. For. Meteorol.*, **87**, 291-300.

Meyn, S. K., 2001: Heat fluxes through roofs and their relevance to estimates of urban heat storage. Ph. D. dissertation, University of British Columbia, 118 pp.

Miao, S. G. and F. Chen, 2014: Enhanced modeling of latent heat flux from urban surfaces in the Noah/single-layer urban canopy coupled model. *Science China Earth Sciences*, **57**, 2408-2416.

Mitchell, V. G., R. G. Mein and T. A. Mcmahon, 2001: Modelling the urban water cycle. *Environmental Modelling & Software*, **16**, 615-629.

Mitchell, V. G., H. A. Cleugh, C. S. B. Grimmond and J. Xu, 2008: Linking urban water balance and energy balance models to analyse urban design options. *Hydrol. Process.*, **22**, 2891–2900.

Monteith, J. L., 1965: Evaporation and environment. *Symp. Soc. Exp. Biol.* **19**, 205–224.

Nakayoshi, M., R. Moriwaki, T. Kawai and M. Kanda, 2009: Experimental study on rainfall interception over an outdoor urban-scale model, *Water Resour. Res.*, **45**, W04415, doi: 10.1029/2008WR007069.

Narita, K., T. Sekine and T. Tokuoka, 1984: Thermal properties of urban surface materials - study on heat balance at asphalt pavement. *Geogr.Rev. Jpn.*, **57**, 639–651.

Nie, W., B. F. Zaitchik, G. Ni and T. Sun, 2017: Impacts of Anthropogenic Heat on Summertime Rainfall in Beijing. *J. Hydrometeor.*, **18**, 693-

712.
Novak, M. D., 1981: The moisture and thermal regimes of a bare soil in the lower fraser valley during spring. Ph. D. dissertation, University of British Columbia, 175 pp.
Ogink-Hendriks, M. J., 1995: Modelling surface conductance and transpiration of an oak forest in the Netherlands. *Agric. For. Meteorol.*, **74**, 99–118.
Oke, T. R., 1988: The urban energy balance. *Prog. Phys. Geogr.* **12**, 471-508.
Oleson, K.W., G. B. Bonan, J. Feddema, M. Vertenstein, C. S. B. Grimmond, 2008: An urban parameterization for a global climate model. Part I: Formulation and evaluation or two cities. *J. Appl. Meteorol. Climatol.* **47**, 1038–1060.
Rafael, S., H. Martins, M. Marta-Almeida, E. Sa, S. Coelho, A. Rocha, C. Borrego and M. Lopes, 2017: Quantification and mapping of urban fluxes under climate change: Application of WRF-SUEWS model to Greater Porto area (Portugal). *Environ. Res.*, **155**, 321-334.
Ragab, R., J. Bromley, P. Rosier, J. D. Cooper and J. H. C. Gash, 2003: Experimental study of water fluxes in a residential area: 1. Rainfall, roof runoff and evaporation: the effect of slope and aspect. *Hydrological Processes*, **17**, 2409–2422.
Roberts, S. M., T. R. Oke, C. S. B. Grimmond and J. A. Voogt, 2006: Comparison of four methods to estimate urban heat storage. *J. Appl. Meteorol. Climatol.*, **45**, 1766–1781.
Roth, M., C. Jansson and E. Velasco, 2017: Multi-year energy balance and carbon dioxide fluxes over a residential neighbourhood in a tropical city. *Int. J. Climatol.*, **37**, 2679–2698.
Salamanca, F., M. Georgescu, A. Mahalov, M. Moustaoui and M. Wang, 2014: Anthropogenic heating of the urban environment due to air conditioning, *J. Geophys. Res. Atmos.*, **119**, 5949–5965.
Sailor, D. J., 2011: A review of methods for estimating anthropogenic heat and moisture emissions in the urban environment. *Int. J. Climatol.*, **31**, 189–199.
Sailor, D. J. and L. Lu, 2004: A top-down methodology for developing diurnal and seasonal anthropogenic heating profiles for urban areas. *Atmos. Environ.*, **38**, 2737–2748.
Sailor, D. J.and C. Vasireddy, 2006: Correcting aggregate energy consumption data to account for variability in local weather. *Environ. Model. Softw.* **21**, 733-738.
Sailor D. J., M. Georgescu, J. M. Milne and M. A. Hart, 2015: Development of a national anthropogenic heating database with an extrapolation for international cities. *Atmos. Environ.*, **118**, 7–18, doi:10.1016/j.atmosenv.2015.07.016.
Shanghai Municipal Statistics Bureau, 2016: Shanghai Statistical Year Book 2016. China Statistics Press: Beijing, China, 473pp. http://www.stats-sh.gov.cn/html/sjfb/201701/1000339.html (last accessed: 30 November 2017)
Shanghai Municipal Statistics Bureau of Xuhui District, 2013: Statistical year book of Xuhui District. http://tjj.xh.sh.cn/site/tjj/m/cnt/?id=1877 (last accessed: 1 December 2017)
Shi, Y., X. Gao, Y. Xu, F. Giorgi and D. Chen, 2016: Effects of climate change on heating and cooling degree days and potential energy demand in the household sector of China. *Clim. Res.*, **67**, 135-149.
Souch, C., C. S. B. Grimmond and C. P. Wolfe, 1998: Evapotranspiration rates from wetlands with different disturbance histories: Indiana dunes National Lakeshore. *Wetlands*, **18**, 216-229.
Stewart, I. D., T. R. Oke, 2012: Local climate zones for urban temperature studies. *Bull. Am. Meteorol. Soc.*, **93**, 1879–1900.
Stewart, I. D. and C. A. Kennedy, 2016: Metabolic heat production by human and animal populations in cities. *Int. J. Biometeor.*, **61**, 1-13.
Stewart, J. B., 1988: Modelling surface conductance of pine forest. *Agric. For. Meteorol.*, **43**, 19–35.
Su, Z., X. Zhi, J. Bian, R. Li and J. Sun, 2014: Research on the influence of precipitation on traffic characteristics of urban expressway in Shanghai (in Chinese). Atmospheric Science Research and Application, 1, 68-76.
Sun, T., E. Bou-Zeid and G. Ni, 2014: To irrigate or not to irrigate: Analysis of green roof performance via a vertically-resolved hygrothermal model. *Building & Environment*, **73**, 127-137.
Sun, T., Z. H. Wang, W. Oechel and C. S. B. Grimmond, 2017: The analytical objective hysteresis model (AnOHM v1.0): methodology to determine bulk storage heat flux coefficients. *Geosci.* Model Dev., 10, 2875–2890.
Takane, Y., Y. Kikegawa, M. Hara, T. Ihara, Y. Ohashi, S. A. Adachi, H. Kondo, K. Yamaguchi and N. Kaneyasu, 2017: A climatological validation of urban air temperature and electricity demand simulated by a regional climate model coupled with an urban canopy model and a building energy model in an Asian megacity. *Int. J. Climatol.*, **37**, 1035-1052.
Tang, Y. Q., J. G. Tan, C. S. B. Grimmond, Y. Chang and X. Ao, 2016: Estimation and analysis of aerodynamic parameters for a typical large city (in Chinese). *Journal of Tropical Meteorology*, **3**, 503-514.
United Nations, Department of Economic and Social Affairs, Population Division, 2017: World Population Prospects: The 2017 Revision, Key Findings and Advance Tables. Working Paper No. ESA/P/WP.227. http://esa.un.org/unpd/wpp/Documentation/pdf/WPP2012_%20KEY%20FINDINGS.pdf
Vahmani, P. and T. S. Hogue, 2014: Incorporating an urban irrigation module into the noah land surface model coupled with an urban canopy model. *J. Hydrometeorol.*, **15**, 1440–1456.
Vahmani, P. and T. S. Hogue, 2015: Urban irrigation effects on WRF-UCM summertime forecast skill over the Los Angeles metropolitan area. *J. Geophys. Res. Atmos.*, **120**, 9869-9881.
Wang, X., J. Liao, J. Zhang, C. Shen, W. Chen, B. Xia, and T. Wang, 2013: A numeric study of regional climate change induced by urban expansion in Pearl River Delta, China, *J. Appl. Meteorol. Climatol.*, **53**, 346–362.
Wang, X, X. Sun, J. Tang, and X. Yang, 2015: Urbanization-induced regional warming in Yangtze River Delta: potential role of anthropogenic heat release. *Int. J. Climatol.*, **35**, 4417-4430.
Ward, H. C., S. Kotthaus, L. Järvi, L. and C. S. B. Grimmond, 2016: Surface urban energy and water balance scheme (SUEWS): Development and evaluation at two UK sites. *Urban Climate*, **18**, 1-32.
Ward, H. C. and C. S. B. Grimmond, 2017a: Assessing the impact of changes in surface cover, human behaviour and climate on energy partitioning across Greater London. *Landscape & Urban Planning*, **165**, 142-161.
Ward, H. C., L. Järvi, S. Onomura, F. Lindberg and C. S. B. Grimmond, 2017b: SUEWS manual: Version 2017. http://urban-climate.net/umep/SUEWS.
Wu, K. and X. -Q. Yang, 2013: Urbanization and heterogeneous surface warming in Eastern China. *Chin. Sci. Bull.* **58**, 1363–1373.
Xu, J., L. Chang, Y. Qu, F. Yan, F. Wang and Q. Fu, 2016: The meteorological modulation on PM2.5 interannual oscillation during 2013 to 2015 in Shanghai, China. *Science of the Total Environment*, **572**, 1138-1149.
Yang, J., Z.-H. Wang, F. Chen, S. Miao, M. Tewari, J. A. Voogt and S. Myint, 2015: Enhancing hydrologic modelling in the coupled Weather Research and Forecasting–urban modelling system. *Bound.-Layer Meteor.*, **155**, 87–109.
Yang, X., L. R. Leung, N. Zhao, C. Zhao, Y. Qian, K. Hu, X. Liu and B. Chen, 2017: Contribution of urbanization to the increase of extreme heat events in an urban agglomeration in east China. *Geophysical Research Letters*, **44**, 6940-6950.
Yu, J. and J. Wen, 2016: Multi-criteria Satisfaction Assessment of the Spatial Distribution of Urban Emergency Shelters Based on High-Precision Population Estimation. *International Journal of Disaster Risk Science*, **7**, 413-429.

Zhang, N., Z. Gao, X. Wang, and Y. Chen, 2010: Modeling the impact of urbanization on the local and regional climate in Yangtze River Delta, China, *Theor. Appl. Climatol.*, **102**, 331–342.

Zhang, N., X. Wang, Y. Chen, W. Dai, and X. Wang, 2015: Numerical simulations on influence of urban land cover expansion and anthropogenic heat release on urban meteorological environment in Pearl River Delta, *Theor. Appl. Climatol.*, **126**, 469-479.

Zhao, H. 2007: The study on the sustainable urban transportation mode: the case study of Shanghai. Ms,c dissertation, East China Normal University, 65pp.

Zhong, S., Y. Qian, C. Zhao, R. Leung and X.-Q. Yang, 2015: A case study of urbanization impact on summer precipitation in the Greater Beijing Metropolitan Area: Urban heat island versus aerosol effects, *J. Geophys. Res. Atmos.*, **120**, 10903-10914, doi:10.1002/2015JD023753.

Zhong, S., Y. Qian, C. Zhao, R. Leung, H. Wang, B. Yang, J. Fan, H. Yan, X. -Q. Yang and D. Liu, 2017: Urbanization-induced urban heat island and aerosol effects on climate extremes in the Yangtze River Delta region of China. *Atmos. Chem. Phys.*, **17**, 1-57.

Zhong W., D. Wang, D Xie and L. Yan, 2017: Dynamic characteristics of Shanghai's population distribution using cell phone signaling data (in Chinese). *Geographical Research*, **36**, 972-984.

Zou, J., B. Zhou and J. Sun, 2017: Impact of eddy characteristics on turbulent heat and momentum fluxes in the urban roughness sublayer. *Bound.-Layer Meteorol.*, **164**, 39-62.

Table 2: Study site (XJH) parameter values used in SUEWS. See text for definitions and sources not given here (Järvi et al. 2011) OHM coefficient (a_1, a_2, a_3) are averages of values from different sources: *Paved*: Doll et al. (1985), Asaeda & Ca (1993), Narita et al. (1984), Anandakumar (1999); *Buildings*: Meyn 2001; *Vegetation*: Fuchs & Hadas (1972), Novak (1981), McCaughey (1985), Asaeda & Ca (1983), Doll et al. (1985); *Bare soil*: Fuchs & Hadas (1972), Novak (1981), Asaeda & Ca (1993); *Water*: Souch et al. (1998). Trees: EveTr – Evergreen, DecTr - Deciduous; Measurement height (z_m).

Location	*Time zone*	$T_{base-on}$ (°C)	$T_{base-off}$ (°C)	GDD_{full} (°C)	SDD_{full} (°C)	*LAI*	*EveTr*	*DecTr*	*Grass*
31.19°N, 21.43°E	UTC+8	10	20	400	-450	*Max*	5.1	5.5	5.9
						Min	4	1	3.2
						c_1		0.04	
						c_2		0.001	
z_m *(m)*	z_H *(m)*	z_0 *(m)*	z_d *(m)*	*Soil depth (mm)*	*Soil Storage Capacity (mm)*	c_3		0.03	
						c_4	10^{-4}	$5*10^{-4}$	$3*10^{-4}$
80	35.9	3.6	25.1	350	150				

	Surface cover							***Irrigation***	
	Paved	*Buildings*	*EveTr*	*DecTr*	*Grass*	*Bare soil*	*Water*		
Fractions	0.62	0.23	0.03	0.01	0.1	0	0.01	*Start - End (DoY)*	1 - 366
a_1 *(-)*	0.719	0.238		0.336		0.355	0.500	$b_{0,m}$ (mm)	-25.36
a_2 *(h)*	0.194	0.427		0.313		0.335	0.210	$b_{1,m}$ (mm K^{-1})	3
a_3 *(W m^{-2})*	-36.6	-16.7		-31.4		-35.3	-39.1	$b_{2,m}$ (mm d^{-1})	1.1

Table 3: SUEWS model performance statistics (cf. observations) by season for sensible heat flux (Q_H), latent heat flux (Q_E) and storage heat flux (ΔQ_S) for 4 experiments (Exp): Exp 1: base scenario without Q_F and irrigation; 2: Q_F modelled without irrigation; and Exp 3-4 are irrigation scenarios. Figures C.1-3 provide the number (N) of 60 minute data points analysed. Statistics and notation are given in Appendix B.

Exp	Sea.	Q_H					Q_E					ΔQ_S				
		$\bar{O}$	R^2	*RMSE*	*MBE*	*MAE*	$\bar{O}$	R^2	*RMSE*	*MBE*	*MAE*	$\bar{O}$	R^2	*RMSE*	*MBE*	*MAE*
1 $Q_{F,0}$ *Noirr*	Win	48.9	0.57	42.6	-10.7	29.7	14.1	0.20	17.5	-6.9	12.1	-17.8	0.77	50.6	4.4	37.0
	Spr	92.7	0.56	73.3	-32.4	50.7	27.5	0.23	34.7	-8.9	23.0	-14.3	0.74	91.4	42	66.6
	Sum	136.7	0.62	111.6	-64.0	72.6	34.2	0.10	51.8	-17.6	34.3	-47.6	0.5	131.4	87.8	97.4
	Aut	75.3	0.64	70.8	-25.5	41.6	32.4	0.27	44.1	-18.9	27.5	-37	0.45	94.1	44.1	61.0
2. $Q_{F,S}$ *Noirr*	Win		0.57	63.2	46.4	52.6		0.18	17.2	-5.3	11.9	114.3	0.86	77.0	-54.5	62.0
	Spr		0.60	66.7	22.9	51.0		0.20	35.5	-9.6	23.0	105.8	0.81	82.8	-12.4	60.2
	Sum		0.68	79.1	6.3	53.4		0.08	52.5	-18.1	34.8	106.9	0.69	92.4	19.2	63.4
	Aut		0.64	68.4	31.8	54.0		0.22	44.7	-18.6	27.8	91.2	0.63	79.9	-13.0	56.0
3. $Q_{F,S}$ *Irr*	Win		0.58	61.6	44.9	51.4		0.19	16.9	-3.7	11.8					
	Spr		0.56	65.9	9.5	48.9		0.23	36.3	3.8	24.5					
	Sum		0.62	101.8	-32.2	62.2		0.15	57.0	18.9	39.7					
	Aut		0.60	68.9	9.5	48.2		0.36	37.0	3.4	24.7					
4. $Q_{F,S}$ *Irr 3dGap*	Win		0.57	62.1	45.3	51.7		0.19	16.9	-4.0	11.8					
	Spr		0.58	65.6	14.4	49.3		0.23	34.9	-1.6	23.5					
	Sum		0.64	89.7	-15.3	56.5		0.16	49.3	3.3	34.0					
	Aut		0.63	67.4	18.3	49.7		0.34	37.7	-5.1	24.3					